공학박사 학위논문

Evaluation of Interfacial Properties of Thin film considering Constraint Effect between Film and Substrate using Flat-end Vickers Indenter

2020 년 08 월

서울대학교 대학원

재료공학부

이 진 우

Abstract

Lee, Jinwoo
Dept. of Materials Science and Engineering
The Graduate School
Seoul National University

Delamination of thin-coating films on substrates has become a critical issue for the reliability of micro- and nanoelectronic devices. Since failures of the interface may eventually lead to total system failure, evaluation of the interface between its film and substrate becomes an important problem and several testing methods such as a scratch test, pull-off test and peel test have been proposed. However, these conventional tests have limitations as a universal test methods because of limitations of the film characteristics and requirements such as specially designed specimen.

In this thesis, nanoindentation test was developed to overcome the limitations of conventional test methods. In general, nanoindentation testing has been widely applied to evaluate the mechanical properties of thin films such as hardness and elastic modulus at small scale. It was initially used only to evaluate hardness and elastic modulus from the

loading/unloading curve of the indentation testing, but has now been extended to evaluate residual stress, tensile, fracture properties and so on. The nanoindentation test has the advantage that local and thin-film properties can be evaluated through only a single indentation, and no specially designed specimen is needed.

When an indentation is made in nanoindentation testing, the amount of elastic-plastic deformation beneath the indent increases as the indentation load increases. In addition, in the case of a thin film, which is a bond-type heterogeneous material, the total amount of work involved in indentation testing can be expressed as the sum of the work in the film, work in the substrate, and work at the interface. The work at the interface generated by indentation testing can be defined as the resistance to interaction between the film and the substrate, which can be expressed as adhesion at the interface. As a result, in order to evaluate the adhesive force at the interface, the work at the interface is evaluated by a quantitative evaluation of the work in the composite film-substrate structure and the work occurring in the film and the substrate in an independent situation.

If a film of differing hardness and elastic modulus is placed on the substrate and the composite structure is indented, the plastic deformation

in the film is expected to differ from the plastic deformation of the substrate. The stress-strain field of the film and substrate can be determined based on elastic-plastic theory, and the expanding spherical cavity model for indentation gives the individual radial strain components. If there is no adhesion between film and substrate, the radial strain profile exhibits strain discontinuity, but if there is strong adhesion between them, the strain continuity will act strongly. Eventually, the strain continuity across the film and the substrate causes the shape of the strain to bend and the deformation geometry will be distorted. In addition, the relatively soft material will be constrained to the hard material side. As a result, the constraint on film and substrate will depend on the degree of adhesion at the interface between the film and the substrate, and the extent of the constraint can be explained by the change in constraint according to indentation testing. It is thus possible to quantitatively evaluate the amount of constraint change through indentation testing on the film and substrate structure system, and to evaluate the adhesion at the interface using this quantitative evaluation.

Keyword: Adhesion strength; Thin-film system; Composite hardness;

Constraint effect; Interfacial properties; Interfacial constraint; Nanoindentation

Student Number: 2010-23197

Contents

LIST OF FIGURES

Chapter 1

Chapter 2

squares); the solid diamond represents the final interpolated Y, E pair. (b) Corresponding values of force and stiffness resulting from simulations using (a); the solid square is average force and stiffness from the experimental data.

Figure 2.13. (a) Schematic for obtaining stress-strain values using cone indentation with various apical angles and (b) stress-strain curve of silicon nitride calculated from cone indentation tests with various apical angles.

Figure 2.14. Dimensionless function Π relating F/d^2 to representative stress corresponding to various representative plastic values: (a) ε_R=0.01, (b) ε_R =0.033, and (c) ε_R =0.29. The representative plastic strain ε_R =0.033 can be identified as the strain value that allows the construction of Π to be independent of the strain-hardening exponent, n.

Chapter 3

Figure 3.1. 4 kinds of situation beneath indenter.

Figure 3-2. Schematic diagram for (a) negative constraint volume change and (b) positive constraint volume change.

Figure 3-3. Load differences due to the interface at negative constraint.

Chapter 4

Chapter 1

INTRODUCTION

Contents

1.1. Objective of the Thesis

As the technology advances, the multifunctional material has been required in a variety of industries. Among them, the thin film has a major role in most of the major industries. Interface is vulnerable to external influences because of bonding of different materials(fig. 1.1). To evaluate the characteristics of the interface is important, because the interface is the most vulnerable part of the thin-film system. Therefore, many researchers have developed a variety of equipment to evaluate quantitatively the adhesion for a long time, and the analysis method were investigated. However, the existed testing method has three significant limitations.

I. Film and substrate effect

Most of the commercially available test methods which arises the effect of the thin film and the substrate elastic/plastic deformation or fracture indispensably. But it fails to clearly resolve the effect of the film and the substrate yet. The main parameter for assessing the adhesion in the scratch test is the critical load. But critical load can be found that has

a tendency similar to the hardness of the film(fig. 1.2). It is necessary to analyze the effect of film and the substrate in order to obtain an accurate adhesion value.

II. Generality of test method

The applicable test method is limited depending on the material characteristic. Tape method can be applied in the bonding strength is smaller than the tape maximum adhesion[1]. Peel test can also be applied to soft film, and the scratch test is also difficult to apply hard film because of a film cracking before the interface delamination(fig. 1.3).

III. Observation of delamination area or crack length

Most of the adhesion evaluation test method is cracking test. So, after the end of the test it is necessary to measurement of delamination area or crack length from the interface with the optical observations at nano-scale. Also need to check the point of interfacial delamination. However, it is very difficult to accurately measure due to the small test

sample and the test area. This can be confirmed from scratch experimental data in Fig. 1.4.

The objective of the current study is to develop a model to quantitatively evaluate adhesive strength through Instrumented indentation testing (IIT) in order to overcome the limitations of conventional evaluation techniques. IIT, which measures penetration load and depth continuously, is widely used to evaluate mechanical properties because it is a simple procedure that is relatively nondestructive and easy to use on small scales. Performing the indentation test generated the elastic/plastic deformation region to a beneath the indenter. When the indentation depth is more than 10% compared to the film thickness occurs the influence of interface and the substrate[2-5]. In other words, the load-displacement curve that includes the effect of the film/substrate/interface can be obtained from the indentation. Approach was theoretically the effect of the interface in the indentation, as mathematically derived for the curve analysis. Finally, the adhesion strength evaluation model was proposed using the indentation test. It was compared with the surface and interfacial cutting tests in order to verify

validity of the proposed model. And adhesion strength model completed the patent and technology transfer for practical use.

1.2. Organization of the Thesis

This thesis has five chapters. The objective and organization of thesis are briefly described in Chapter 1. Chapter 2 discusses the previous adhesion measurement methods and pointed out the limitations. It also goes into the origin of instrumented indentation tests at nano-scale and the basics of its use to evaluate various mechanical properties. Chapter 3, a theoretical adhesion evaluation model was proposed. Necessary for development of the model, review the formulated hardness and analyzed the effect of interface constraint. Deriving a interface parameter for evaluating the degree of constraint volume. Deriving the final equation using indentation test and physical meaning of the model was investigated. Also, Define the key parameter in the assessment model. Introduction of nanoindentation equipment and experimental work to verify this model are described in Chapter 5. Finally, Chapter 6 summarizes the primary findings of this study.

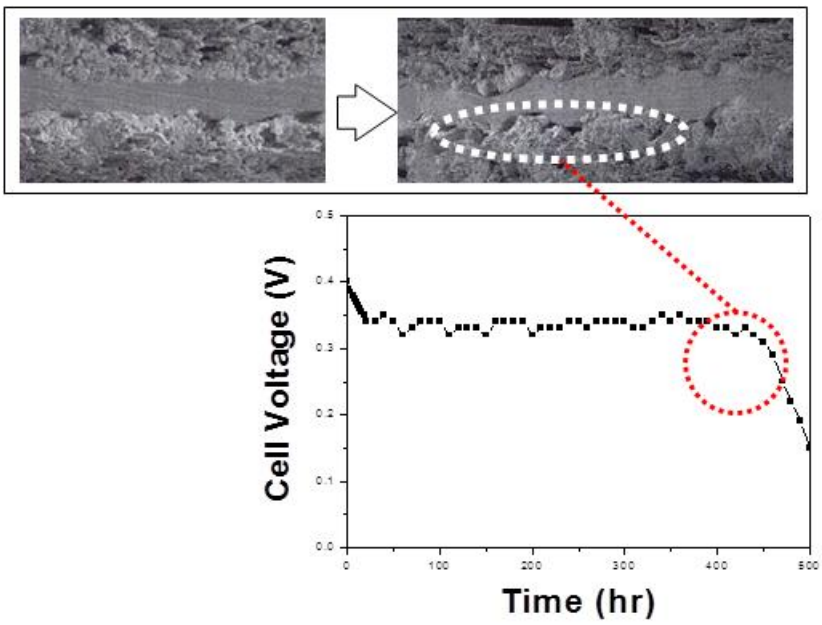

Figure 1.1. Reliability issues caused by interfacial delamination.

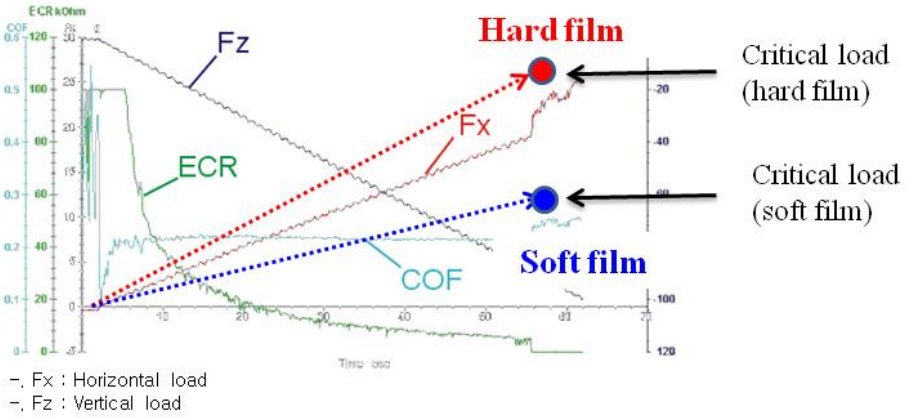

Figure 1.2. Effect of thinfilm in the scratch test

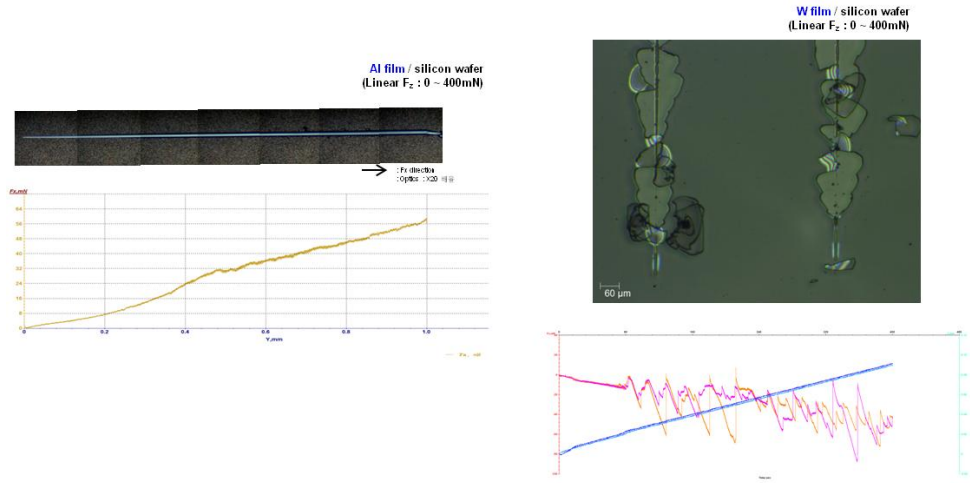

Figure 1.3. Applicability of the material in the scratch test:

(a) Soft film and (b) Hard film

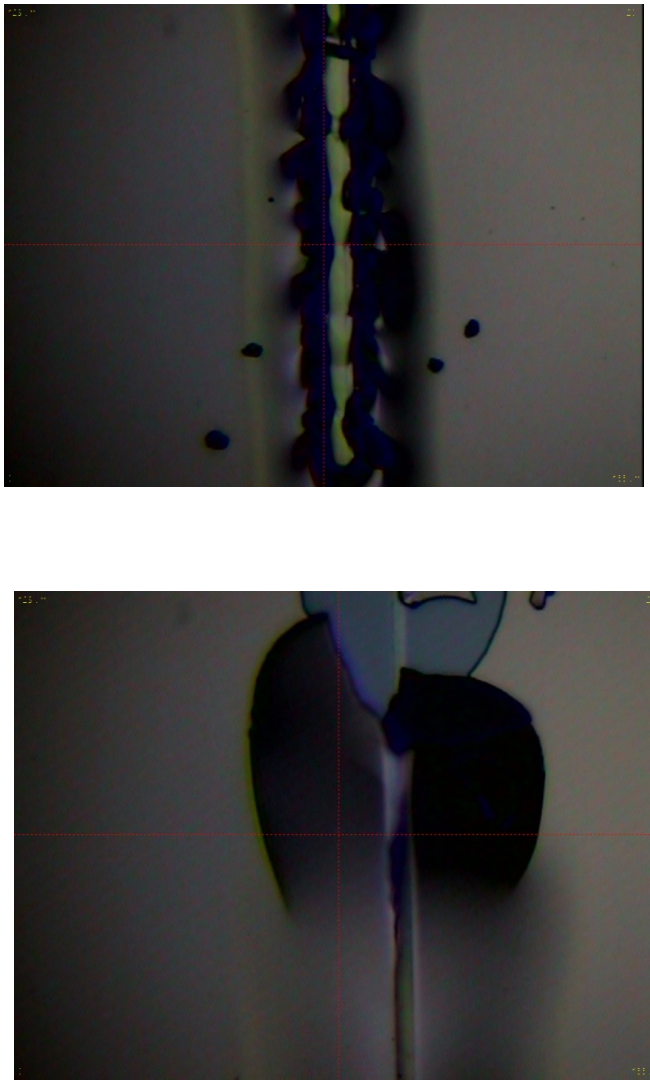

Figure 1.4. The optical image after the scratch test

Chapter 2

RESEARCH BACKGROUND

Contents

2.1. Methods for measuring adhesion

Ideal testing methods are quantitative, have easy-to-prepare samples, and are relevant to real applications. Of the more than a hundred methods for measuring adhesion employing different sample geometries, very few are ideal. This passage surveys some of the most commonly used adhesion evaluation methods. These methods can be divided into various types: destructive or nondestructive, force or energy approach, and quantitative or qualitative.

2.1.1. True work of adhesion

The true work of adhesion is often determined by contact angle measurements[6,7]. If the tested material particle is in thermal equilibrium on a substrate, then:

$$\gamma_{fs} = \gamma_s - \gamma_f \cdot \cos\theta \qquad (2\text{-}1)$$

Where θ is the contact angle between the particle free surface and the substrates. Hence the work of adhesion is given in the following equation:

$$W_{TA} = \gamma_f - \gamma_s - \gamma_{fs} = \gamma_f (1 + \cos\theta) \qquad (2\text{-}2)$$

Droplets in themodynamic equilibrium can be obtained by the sessile drop method[8] or by annealing[6,7]. When the surface energy of the film γ_f is known at a given temperature T_0, at any temperature T, it becomes:

$$\gamma_f(T) \approx \gamma_f(T_0) + (T - T_0)\left(\frac{\partial \gamma_f}{\partial T}\right)_{T=T_0} \qquad (2\text{-}3)$$

Solving Eq. (2-2) and (2-6) for the annealing temperature gives the value of the true(thermodynamic) adhesion energy. In most cases annealing must be performed in vacuum in order to avoid oxidation. If crystallographic faceting occurs upon cooling, a different technique is used to assess the work of adhesion that is based on the aspect ratio measurements of the equilibrated crystals. Contact angle distribution can be obtained from SEM or AFM image analysis. Usually both results; contact angle and aspect ratio measurements agree well for metallic films. The true work of adhesion is a constant for a given film/substrate pair, and for metals on ceramic is typically a small number on the order of 0.5-2 J/m^2.

2.1.2. Practical Work of Adhesion

There are many different methods for measuring adhesion by the fracture-mechanical approach, most of them using some driving force or stored in the material debonding. The energy may come from an external mechanical force imposed on the materials, or it come be stored in the material itself (through the internal material stress). These testing methods generally measure critical values of applied stress intensity K_i or strain energy released rate G_i, Where i can be mode I, II, III, or of mixed character. Below we focus in particular on testing methods appropriate for thin film adhesion.

(1) Superlayer test: A test based upon internally developed stresses proposed by Bagchi and coworkers [9] in which residual tensile stresses in a thin film line drive its delamination from a thick substrate. After crack initiation, the strain energy released rate G is:

$$E_f G = (1-\upsilon_f)\sigma_r{}^2 h_f \qquad (2\text{-}4)$$

where E_f, υ_f, and $\sigma_r{}^2$ are the Young's modulus, Poisson's ratio, and residual stress in the thin film, respectively. It is the non-dimensional

steady state for a marrow line, while the residual stress is biaxial for a wide line (line width greater than line thickness). For a typical film thickness (1um) and residual stress (100MPa), the stress-induced energy released rate is too small, on the order of 0.1 J/m^2. Most interface in microelectronic devices have higher de-bond energies, and this method is difficult to apply under these conditions. In addition, although this method gives comparatively accurate adhesion values, the testing technique is rather tedious and complicated.

(2) Indentation test: The indentation technique is normally used for measuring thin film mechanical properties such as elastic modulus and hardness, and is also useful for modeling the film fracture behavior. Generally, it is known that only for a brittle and weakly bonded film, this method can be used to delaminate the film from the substrate and to measure the interfacial strength [10-11]. Marshall and Evans [11] provide an analysis for conical (plane-stress) indentation-induced thin film delamination. The strain energy released rate is:

$$\frac{E_f G}{(1-\nu_f)} = \frac{\sigma_1^{\,2} h(1-\nu_f)}{2} + h(1-\alpha)[\sigma_R^{\,2} - (\sigma_1 - \sigma_B)^2] \qquad (2\text{-}5)$$

where h is the film thickness, σ_B is the bucking stress in the film, and

α is the slope of the buckling load versus the edge displacement (α=0 if the film does not buckle). Unfortunately, the indentation test can only rarely be used to test adhesion of ductile films on brittle substrates, since a ductile strongly adhered film most often deforms before delamination from the substrate, and even if it debonds from substrate, it does go in a way that is not reproducible.

(3) Scratch test: In a typical scratch test a stylus or a diamond tip is drawn across the film surface. The test can be treated as a combination of two operations: vertical indentation and horizontal tip motion. A vertical increasing load is applied to the tip during scratching until the coating detaches from the substrate. The minimum critical load P_{cr} at which delamination occurs is used as a measure of the practical work of adhesion [12-13]:

$$P_{cr} = \frac{\pi r^2}{2}\left(\frac{2EW_{PA}}{h}\right)^{\frac{1}{2}} \tag{2-6}$$

where r is the contact radius and W_{PA} is the practical work of adhesion. This analysis is applicable only when the tensile stress normal to the film surface drives delamination. Venkataraman et al. developed a model for estimating the energy G per unit area stored in the film from

the scratch elastic distribution [14-15], which was later modified to take into account residual stress in the film [16]:

$$G = \frac{\sigma_R{}^2 h(1-\nu^2)}{2E} + \sum \left(\frac{\tau_{ij}{}^2 h(1-\nu^2)}{2\mu} + \frac{\sigma_{ij}{}^2 h(1-\nu^2)}{2E} \right) \qquad (2\text{-}7)$$

where τ_{ij} and σ_{ij} are the average elastic shear and normal stresses in the delaminated film, and μ is the film shear modulus. This method has the inconvenience that τ_{ij} and σ_{ij} should be determined from the scratch-trace geometry observed in SEM.

(4) Sandwich specimen test: Among the many different sandwich sample geometries, the most common and simplest thing is the modified K_{IC} specimen [17-18], in which a thin film is bonded between the two pieces of a compact tension sample. Another version of this test is the double cantilever test, in which a thin film is bonded between the two rigid elastic plates. For the K_{IC} test, the applied stress intensity can be expressed in the form:

$$K = \frac{P_Q}{B\sqrt{W}} f(a/W) \qquad (2\text{-}8)$$

where P_Q is the load determined from the load-displacement curve, B is

the specimen thickness, W is the specimen width ad defined in Fig 2.1(d), and $f(a/W)$ is a function of a and W that is defined in the standard for the homogeneous material[19].

(5) Bulge and blister test: This method is analogous to uniaxial tension for bulk materials and has been developed for measuring thin film mechanical properties. In this test a freestanding thin film "window" is pressurized on one side, causing it to deflect (Fig. 2.1(e)). The stress-strain curve is constructed from the measured pressure P and film deflection δ, and the pressure-deflection curve is a function of sample geometry, mechanical properties and residual stress. A spherical cap model was initially used for stress and strain determination in the bulge test [20].

$$\sigma = \frac{P \cdot r^2}{4\delta h} \; and \; \varepsilon = \frac{\delta^2}{3r^2} + A \qquad (2\text{-}9)$$

where δ is total bulge height, r is the bulge radius, and A is a term taking into account the initial stress in the film. This method is often invalid for thin ductile films because they yield before uniformly along the perimeter of the blister, making the results difficult to interpret.

2.2. Instrumented indentation tests

There has been considerable recent interest in the mechanical characterization of thin film systems and small volumes of material using depth-sensing indentation tests with either spherical or pyramidal indenters. Usually, the principal goal of such testing is to extract hardness and elastic modulus of the specimen material from experimental readings of indenter load and depth of penetration. These readings give an indirect measure of the area of contact at full load, from which the mean contact pressure, and thus hardness, may be estimated. The test procedure, for both spheres and pyramidal indenters, usually involves an elastic-plastic loading sequence followed by an unloading. The validity of the results for hardness and modulus depends largely upon the analysis procedure used to process the raw data. Such procedures are concerned not only with the extraction of hardness and modulus, but also with correcting the raw data for various systematic errors that have been identified for this type of testing. The forces involved are usually in the mN range and are measured with a resolution of a few nN. The depths of penetration are on the order of microns with a resolution of less than a nanometer.

2.2.1. Elastic Contact mechanics

The stresses and deflections arising from the contact between two elastic solids are of particular interest to those undertaking indentation testing. The most well known scenario is the contact between a rigid sphere and a flat surface as shown in Fig. 2.2.

Hertz found that the radius of the circle of contact a is related to the indenter load *P*, the indenter radius *R*, and the elastic properties of the contacting materials by [21,22]

$$a^3 = \frac{3}{4}\frac{PR}{E_r} \qquad (2\text{-}10)$$

where the quantity E_r combines the modulus of the indenter and the specimen and is given by

$$\frac{1}{E_r} = \frac{1-\nu^2}{E} + \frac{1-\nu_i^{\,2}}{E_i} \qquad (2\text{-}11)$$

where the primed terms apply to the indenter properties. E_r is often referred to as the reduced modulus or combined modulus, of the system. If both contacting bodies have a curvature, then *R* in the above equations is their relative radii given by

$$\frac{1}{R} = \frac{1}{R_1} + \frac{1}{R_2} \qquad (2\text{-}12)$$

In Eq. (2-12), we set the radius of the indenter to be positive always, and the radius of the specimen to be positive if its center of curvature is on the opposite side of the lines of contact between the two bodies.

It is important to realize that the deformations at the contact are localized and the Hertz equations are concerned with these and not the bulk deformations and stresses associated with the method of support of the contacting bodies. The deflection h of the original free surface in the vicinity of the indenter is given by

$$h = \frac{1}{E_r}\frac{3}{2}\frac{P}{4a}\left(2 - \frac{r^2}{a^2}\right), \text{ where } \; r \geq a \qquad (2\text{-}13)$$

It can be easily shown from Eq. (2-13) that the depth of the circle of contact beneath the specimen free surface is half of the total elastic displacement. That is, the distance from the specimen free surface to the depth of the radius of the circle of contact at full load is $h_d = h_c = h_{max}/2$.

The distance of mutual approach of distant points in the indenter and specimen is calculated from

$$\delta^3 = \left(\frac{3}{4E_r}\right)^2 \frac{P^2}{R} \qquad (2\text{-}14)$$

Substituting Eq. (2-13) into Eq. (2-14), we can express the distance of mutual approach as

$$\delta = \frac{a^2}{R} \qquad (2\text{-}15)$$

For the case of a non-rigid indenter, if the specimen is assigned a modulus of E_r, then the contact can be viewed as taking place between a rigid indenter of radius R and the specimen. in Eq. (2-14) becomes the total depth of penetration h_{max} beneath the specimen free surface. Rearranging Eq. (2-14) slightly, we obtain

$$P = \frac{4}{3} E_r R^{1/2} h_{\max}{}^{3/2} \qquad (2\text{-}16)$$

Although the substituting of E_r for the specimen modulus and the associated assumption of a rigid indenter of radius R might satisfy the contact mechanics of the situation by Eq. (2-10) to Eq. (2-16), it should be realized that for the case of a non-rigid indenter, the actual deformation experienced by the specimen is that obtained with a contact with a rigid indenter of a larger radius R^+ as shown in Fig. 2.4. This larger radius may be computed using Eq. (2-10) with E_i in Eq. (2-11) set as for a rigid indenter. In terms of the radius of the contact circle a, the equivalent rigid indenter radius is given by [23]

$$R^{+} = \frac{4a^3 E}{3(1-\nu^2)P} \tag{2-17}$$

The mean contact pressure, P_m, is given by the indenter load divided by the contact area and is a useful normalizing parameter, which has the additional virtue of having actual physical significance:

$$P_m = \frac{P}{\pi a^2} \tag{2-18}$$

Combining Eq. (2-10) and (2-18), we obtain

$$p_m = \left(\frac{4E_r}{3\pi}\right)\frac{a}{R} \tag{2-19}$$

We may refer to the mean contact pressure as the indentation stress, and the quantity a/R as the indentation strain. This functional relationship between P_m and a/R foreshadows the existence of a stress-strain response similar in nature to that more commonly obtained from conventional uniaxial tension and compression tests. In both cases, a fully elastic condition yields a linear response. However, owing to the localized nature of the stress field, an indentation stress-strain relationship yields valuable information about the elastic-plastic properties of the test material that is not generally available from uniaxial tension and compression tests, especially for brittle materials.

For a conical indenter, similar equations apply where the radius of circle of contact is related to the indenter load by [24]

$$P = \frac{\pi a}{2} E_r a \cdot \cot \alpha \qquad (2\text{-}20)$$

The depth profile of the deformed surface within the area of contact is

$$h = \left(\frac{\pi}{2} - \frac{r}{a} \right) a \cdot \cot \alpha \text{, where } \; r \le a \qquad (2\text{-}21)$$

is the cone semi-angle as shown in Fig. 2.4. The quantity $a \cdot \cot \alpha$ is the depth of penetration h_c measured at the circle of contact. Substituting Eq. (2-20) into Eq. (2-21) with r=0, we obtain

$$P = \frac{2E \cdot \tan \alpha}{\pi} h_c^{\,2} \qquad (2\text{-}22)$$

where h_c is the depth of penetration of the apex of the indenter beneath the original specimen free surface.

In indentation testing, the most common types of indenters are spherical indenters, where the Hertz equations apply directly, or pyramidal indenters. The most common types of pyramidal indenters are the four-sided Vickers indenter and the three-sided Berkovich indenter. Of particular interest in indentation testing is the area of the contact found from the dimensions of the contact perimeter. For a spherical indenter, the radius of the circle of contact is given by

$$a = \sqrt{2R_i^2 h_c - h_c^2} = \sqrt{2R_i h_c}\,, \qquad (2\text{-}23)$$

where h_c is the depth of the circle of contact as shown in Fig. 2.2. The approximation of Eq. (2-23) is precisely that which underlies the Hertz equations (Eqs. (2-10) and (2-13)) and thus these equations apply to cases where the deformation is small, that is, when the depth h_c is small in comparison to the radius R_i.

For a conical indenter, the radius of the circle of contact is simply

$$a = h_c \cdot \tan\alpha \qquad (2\text{-}24)$$

In indentation testing, pyramidal indenters are generally treated as conical indenters with a cone angle that provides the same area to depth relationship as the actual indenter in question. This allows the use of convenient axial symmetric elastic equations, Eqs. (2-20) to (2-22), to be applied to contacts invoking non-axial-symmetric indenters. Despite the availability of contact solutions for pyramidal punch problems [25,26], the conversion to an equivalent axial-symmetric has found a wide acceptance. The areas of contact as a function of the depth of the circle of contact for some common indenter geometries are given in Table 2.1 along with other information to be used in the analysis methods.

2.2.2. Elastic-Plastic Contact mechanics

Indentation tests on many materials result in both elastic and plastic deformation of the specimen material. In brittle materials, plastic deformation most commonly occurs with pointed indenters such as the Vickers diamond pyramid. In ductile materials, plasticity may be readily induced with a blunt indenter such as a sphere or cylindrical punch. Indentation tests are used routinely in the measurement of hardness of materials, but Vickers, Berkovich, and Knoop diamond indenters may be used to investigate other mechanical properties of solids such as specimen strength, fracture toughness, and internal residual stresses. The meaning of hardness has been the subject of considerable attention by scientists and engineers since the early l700s. It was appreciated very early on that hardness indicated a resistance to penetration or permanent deformation. Early methods of measuring hardness, such as the scratch method, although convenient and simple, were found to involve too many variables to provide the means for a scientific definition of hardness. Static indentation tests involving spherical or conical indenters were first used as the basis for theories of hardness. Compared to dynamic tests, static tests enabled various criteria of hardness to be established since the

number of test variables was reduced to a manageable level. The most well-known criterion is that of Hertz, who postulated that an absolute value for hardness was the least value of pressure beneath a spherical indenter necessary to produce a permanent set at the center of the area of contact. Later treatments by Auerbach [27], Meyer [28] and Hoyt [29] were all directed to removing some of the practical difficulties in Hertz's original proposal.

- **Constraint Factor**

Static indentation hardness tests usually involve the application of load to a spherical or pyramidal indenter. The pressure distribution beneath the indenter is of particular interest. The value of the mean contact pressure P_m at which there is no increase with increasing indenter load is shown by experiment to be related to the hardness number H. For hardness methods that employ the projected contact area, the hardness number H is given directly by the mean pressure P_m at this limiting condition. Experiments show that the mean pressure between the indenter and the specimen is directly proportional to the material's yield, or flow stress in compression, and can be expressed as

$$H \approx CY \tag{2-25}$$

where Y is the yield, or flow stress, of the material. The mean contact pressure in an indentation test is higher than that required to initiate yield in a uniaxial compression test because it is the shear component of stress that is responsible for plastic flow. The maximum shear stress is equal to half the difference between the maximum and minimum principal stresses, and in an indentation stress field, where the stress material is constrained by the surrounding matrix, there is a considerable hydrostatic component-Thus, the mean contact pressure is greater than that required to initiate yield when compared to a uniaxial compressive stress. It is for this reason that C in Eq. (2-25) is called the constraint factor, the value of which depends upon the type of specimen, the type of indenter, and other experimental parameters. For the indentation methods mentioned here, both experiments and theory predict C=3 for materials with a large value of the ratio E/Y (e.g., metals). For low values of E/Y (e.g., glasses [30,31]), C≈l.5. The flow, or yield stress Y, in this context is the stress at which plastic yielding first occurs.

- **Indentation Response of Materials**

A material's hardness value is intimately related to the mean contact pressure P_m beneath the indenter at a limiting condition of

compression. Valuable information about the elastic and plastic properties of a material can be obtained with spherical indenters when the mean contact pressure, or indentation stress, is plotted against the indentation strain a/R. The indentation stress-strain response of an elastic-plastic solid can generally be divided into three regimes, which depend on the uniaxial compressive yield stress Y of the material [82]:

l. $P_m < 1.1Y$: full elastic response, no permanent or residual impression left in the test specimen after removal of load.

2. $1.1Y < P_m < CY$: plastic deformation exists beneath the surface but is constrained by the surrounding elastic material, where C is a constant whose value depends on the material and the indenter geometry.

3. $P_m = CY$: plastic region extends to the surface of the specimen and continues to grow in size such that the indentation contact area increases at a rate that gives little or no increase in the mean contact pressure for further increases in indenter load.

In Region 1, during the initial application of load, the response is elastic and can be predicted from Eq. (2-19). Eq. (2-19) assumes linear elasticity and makes no allowance for yield within the specimen material. For a fully elastic response, the principal shear stress for indentation with a spherical indenter is a maximum at $\approx 0.47\ P_m$ at a depth of $\approx 0.5a$ beneath

the specimen surface directly beneath the indenter [32]. Following Tabor [82], we may employ either the Tresca or von Mises shear stress criteria, where plastic flow occurs at $\tau \approx 0.5Y$, to show that plastic deformation in the specimen beneath a spherical indenter can be first expected to occur when $P_m \approx 1.1Y$. Theoretical treatment of events within Region 2 is difficult because of the uncertainty regarding the size and shape of the evolving plastic zone. At high values of indentation strain (Region 3), the mode of deformation appears to depend on the type of indenter and the specimen material. The presence of the free surface has an appreciable effect, and the plastic deformation within the specimen is such that, assuming no work hardening, little or no increase in P_m occurs with increasing indenter load.

- **Hardness Theories**

Theoretical approaches to hardness can generally be categorized according to the characteristics of the indenter and the response of the specimen material. Various semiempirical models that describe experimentally observed phenomena at values of indentation strain at or near a condition of full plasticity have been given considerable attention in the literature [31,33-45,82]. These models variously describe the

response of the specimen material in terms of slip lines, elastic displacements, and radial compressions. For sharp wedge or conical indenters, substantial upward flow is usually observed, and because elastic strains are thus negligible compared to plastic strains, the specimen can be regarded as being rigid plastic. A cutting mechanism is involved, and new surfaces are formed beneath the indenter as the volume displaced by the indenter is accommodated by the upward flow of plastically deformed material. The constraint factor C in this case arises due to flow and velocity considerations [34]. For blunt indenters, the specimen responds in an elastic-plastic manner, and plastic flow is usually described in terms of the elastic constraint offered by the surrounding material. With blunt indenters, Samuels and Mulhearn [37] noted that the mode of plastic deformation at a condition of full plasticity appears to be a result of compression rather than cutting, and the displaced volume is assumed to be taken up entirely by elastic strains within the specimen material. This idea was given further attention by Marsh [36], who compared the plastic deformation in the vicinity of the indenter to that which occurs during the radial expansion of a spherical cavity subjected to internal pressure, an analysis of which was given previously by Hill [35]. The most widely accepted treatment is that of

Johnson [33,39-45], who replaced the expansion of the cavity with that of an incompressible hemispherical core of material subjected to an internal pressure. Here, the core pressure is directly related to the mean contact pressure. This is the so-called expanding cavity model. In the expanding cavity model, the contacting surface of the indenter is encased by a hydrostatic core of radius a_c, which is in turn surrounded by a hemispherical plastic zone of radius c as shown in Fig. 2.5. An increment of penetration dh of the indenter results in an expansion of the core d_a and the volume displaced by the indenter is accommodated by radial movement of particles $du(r)$ at the core boundary. This in turn causes the plastic zone to increase in radius by an amount dc.

For geometrically similar indentations, such as with a conical indenter, the radius of the plastic zone increases at the same rate as that of the core, hence, $da/dc = a/c$.

Using this result Johnson shows that the pressure in the core can be calculated from

$$\frac{p}{Y} = \frac{2}{3}\left[1 + \ln\left(\frac{(E/Y)\tan\beta + 4(1-2\nu)}{6(1-\nu^2)}\right)\right] \qquad (2\text{-}26)$$

where p is the pressure within the core and β is the angle of inclination of the indenter with the specimen surface.

The mean contact pressure is found from

$$p_m = p + \frac{2}{3}Y \tag{2-27}$$

and this leads to a value for the constraint factor *C*. When the free surface of the specimen begins to influence appreciably the shape of the plastic zone, and the plastic material is no longer elastically constrained, the volume of material displaced by the indenter is accommodated by upward flow around the indenter. The specimen then takes on the characteristics of a rigid-plastic solid, because any elastic strains present are very much smaller than the plastic flow of unconstrained material. Plastic yield within such a material depends upon a critical shear stress, which may be calculated using either of the von Mises or Tresca failure criteria. In the slip-line field solution, developed originally in two dimensions by Hill, Lee, and Tupper [34], the volume of material displaced by the indenter is accounted for by upward flow, as shown in Fig. 2.6.

The material in the region ABCDE Rows upward and outward as the indenter moves downward under load. Because frictionless contact is assumed, the direction of stress along the line AB is normal to the face of the indenter. The lines within the region ABDEC are oriented at 45° to

AB and are called slip lines (lines of maximum shear stress). This type of indentation involves a cutting of the specimen material along the line OA and the creation of new surfaces that travel upward along the contact surface. The contact pressure across the face of the indenter is given by

$$p_m = 2\tau_{\max}(1+\alpha) = H \tag{2-28}$$

where τ_{max} is the maximum value of shear stress in the specimen material and α is the cone semi-angle (in radians).

Invoking the Tresca shear stress criterion, where plastic flow occurs at $\tau_{max} = 0.5Y$, and substituting into Eq. (2-28), gives

$$H = Y(1+\alpha)\text{, where } \quad C = (1+\alpha). \tag{2-29}$$

The constraint factor determined by this method is referred to as C_{flow}. For values of between 70° and 90°, Eq. (2-27) gives only a small variation in C_{flow} of 2.22 to 2.7. Friction between the indenter and the specimen increases the value of C_{flow}. A slightly larger value for C_{flow} is found when the von Mises stress criterion is used (where $\tau_{max} \approx 0.58Y$). For example, at α = 90°, Eq. (2-27) with the von Mises criterion gives C = 3.

2.3. Nanoindentation

2.3.1. Development

The present field of nanoindentation grew from a desire to measure the mechanical properties of hard thin films and other near surface treatments in the early 1980s. Microhardness testing instruments available at the time could not apply low enough forces to give penetration depths less than the required 10% or so of the film thickness so as to avoid influence on the hardness measurement from the presence of the substrate. Even if they could, the resulting size of the residual impression cannot be determined with sufficient accuracy to be useful. For example, the uncertainty in a measurement of a 5 μm diagonal of a residual impression made by a Vickers indenter is on the order of 20% when using an optical method and increases with decreasing size of indentation and can be as high as 100% for a 1 μm impression.

Since the spatial dimensions of the contact area are not conveniently measured, modern nanoindentation techniques typically use the measured depth of penetration of the indenter and the known geometry of the indenter to determine the contact area. Such a procedure is sometimes

called depth-sensing indentation testing. For such a measurement to be made, the depth measurement system needs to be referenced to the specimen surface, and this is usually done by bringing the indenter into contact with the surface with a very small initial contact force, which, in turn, results in an inevitable initial penetration of the surface by the indenter that must be accounted for in the analysis. Additional corrections are required to account for irregularities in the shape of the indenter, deflection of the loading frame, and piling-up of material around the indenter. These effects contribute to errors in the recorded depths and, subsequently, the hardness and modulus determinations. Furthermore, the scale of deformation in a nanoindentation test becomes comparable to the size of material defects such as dislocations and grain sizes, and the continuum approximation used in the analysis can become less valid.

The nanoindentation test results provide information on the elastic modulus, hardness, strain-hardening, cracking, phase transformations, creep, and energy absorption. The sample size is very small and the test can in many cases be considered non-destructive. Specimen preparation is straightforward. Because the scale of deformation is very small, the technique is applicable to thin surface films and surface modified layers. In many cases, the microstructural features of a thin film or coating

differs markedly from that of the bulk material owing to the presence of residual stresses, preferred orientations of crystallographic planes, and the morphology of the microstructure. The applications of the technique therefore cover technologies such as cathodic are deposition, physical vapor deposition (PVD), and chemical vapor deposition (CVD) as well as ion-implantation and functionally graded materials. Nanoindentation instruments are typically easy to use, operate under computer control, and require no vacuum chambers or other expensive laboratory infrastructure. The technique relies on a continuous measurement of depth of penetration with increasing load and appears to be have first demonstrated by Pethica [46] in 1981 and was applied to the measurement of the mechanical properties of ion-implanted metal surfaces, a popular application of the technique for many years [47]. The notion of marking use of the elastic recovery of hardness impressions to determine mechanical properties is not a new one, being reported in 1961 by Stillwell and Tabor [48], and also by Lawn and Howes [49] in 1981. The present modern treatments probably begin with Bulychev, Alekhin, Shorshorov, and Ternovskii [50] , who in 1975 showed how the area of contact could be measured using the unloading portion of the load-displacement curve. Loubet, Georges, Marchesini, and Meille [51] used

this method for relatively high load testing (in the order of 1 N) and Doerner and Nix [83] extended the measurements into the mN range in 1986. The most commonly used method of analysis is a refinement of the Doerner and Nix approach by Oliver and Pharr [84] in 1992. A complementary approach directed to indentations with spherical indenters was proposed by Field and Swain and coworkers [52,53] in 1993 and was subsequently shown to be equivalent to the Oliver and Pharr method [54]. Review articles [55,56] on micro, and nanoindentation show a clear evolution of the field from traditional macroscopic measurements of hardness. The field now supports specialized symposia on an annual basis attracting papers covering topics from fundamental theory to applications of the technique.

The first ultramicro hardness tests were done with apparatus designed for use inside the vacuum chamber of a scanning electron microscope (SEM), where load was applied to a sharply pointed tungsten wire via the movement of a galvanometer that was controlled externally by electric current. Depth of penetration was determined by measuring the motion of the indenter support using an interferometric method. The later use of strain gauges to measure the applied load and finely machined parallel springs operated by an electromagnetic coil bought the measurement

outside the vacuum chamber into the laboratory, but, although the required forces could now be applied in a controlled manner, optical measurements of displacement or sizes of residual impressions remained a limiting factor. Developments in electronics lead to the production of displacement measuring sensors with resolutions greater than those offered by optical methods and, in the last ten years, some six or seven instruments have evolved into commercial products, often resulting in the creation of private companies growing out of research organizations to sell and support them. There is no doubt that as the scale of mechanisms becomes smaller, interest in mechanical properties on a nanometer scale and smaller, and the nature of surface forces and adhesion, will continue to increase. Indeed, at least one recent publication refers to the combination of a nanoindenter and an atomic force microscope as a picoindenter [57] suitable for the study of pre-contact mechanics, the process of making contact, and actual contact mechanics. The present maturity of the field of nanoindentation makes it a suitable technique for the evaluation of new materials technologies by both academic and private industry research laboratories and is increasingly finding application as a quality control tool.

2.3.2. Application

- **Hardness and Elastic Modulus**

A schematic representation of a typical data set obtained with a Berkovich indenter is presented in Fig. 2.7, where the parameter P designates the load and h the displacement relative to the initial un-deformed surface. For modeling purposes, deformation during loading is assumed to be both elastic and plastic in nature as the permanent hardness impression forms. During unloading, it is assumed that only the elastic displacements are recovered; it is the elastic nature of the unloading curve that facilitates the analysis. For this reason, the method does not apply to materials in which plasticity reverses during unloading. However, finite element simulations have shown that reverse plastic deformation is usually negligible [58].

There are three important quantities that must be measured from the P-h curves: the maximum load, P_{max}, the maximum displacement, h_{max}, and the elastic unloading stiffness, $S=dP/dh$, defined as the slope of the upper portion of the unloading curve during the initial stages of unloading (also called the contact stiffness). The accuracy of hardness and modulus measurement depends inherently on how well these parameters can be

measured experimentally. Another important quantity is the final depth, h_f, the permanent depth of penetration after the indenter is fully unloaded.

The analysis used to determine the hardness, H, and elastic modulus, E, is essentially an extension of the method proposed by Doerner and Nix [83] that accounts for the fact that unloading curves are distinctly curved in a manner that cannot be accounted for by the flat punch approximation. In the flat punch approximation used by Doerner and Nix, the contact area remains constant as the indenter is withdrawn, and the resulting unloading curve is linear. In contrast, experiments have shown that unloading curves are distinctly curved and usually well approximated by the power law relation

$$P = \alpha\left(h - h_f\right)^m, \qquad (2\text{-}30)$$

where α and m are power law fitting constants [84].

The exact procedure used to measure H and E is based on the unloading processes shown schematically in Fig. 2.8, in which it is assumed that the behavior of the Berkovich indenter can be modeled by a conical indenter with a half-included angle, , that gives the same depth-to-area relationship, =70.3°. The basic assumption is that the contact periphery sinks-in in a manner that can be described by models for

indentation of a flat elastic half-space by rigid punches of simple geometry [59-63]. This assumption limits the applicability of the method since it does not account for the pile-up of material at the contact periphery that occurs in some elastic-plastic materials. Assuming, however, that pile-up is negligible, the elastic models show that the amount of sink-in, h_d, is given by

$$h_d = \varepsilon \frac{P_{\max}}{S}, \qquad (2\text{-}31)$$

where is a constant that depends on the geometry of the indenter. Important values are: =0.72 for a conical punch, =0.75 for a paraboloid of revolution (which approximates to a sphere at small depths), and =1.00 for a flat punch [59].

Using Eq. (2-31) to approximate the vertical displacement of the contact periphery, it follows from the geometry of Fig. 2.8 that the depth along which contact is made between the indenter and the specimen, $h_c = h_{max} - h_d$, is

$$h_c = h_{\max} - \varepsilon \frac{P_{\max}}{S}. \qquad (2\text{-}32)$$

Letting $F(d)$ be an area function that describes the projected (or cross-sectional) area of the indenter at a distance d back from its tip, the

contact area A is then

$$A = F(h_c). \tag{2-33}$$

The area function, also sometimes called the indenter shape function, must be carefully calibrated by independent measurements so that deviations from non-ideal indenter geometry are taken into account. These deviations can be quite severe near the tip of the Berkovich indenter, where some rounding inevitably occurs during the grinding process.

Once the contact area is determined, the hardness is estimated from

$$H = \frac{P_{\max}}{A}. \tag{2-34}$$

Note that because this definition of hardness is based on the contact area under load, it may deviate from the traditional hardness measured from the area of the residual hardness impression if there is significant elastic recovery during unloading. However, this is generally important only in materials with extremely small values of E/H [85].

Measurement of the elastic modulus follows from its relationship to contact area and the measured unloading stiffness through the relation

$$S = \beta \frac{2}{\sqrt{\pi}} E_r \sqrt{A} \tag{2-35}$$

where E_r is the reduced modulus as in the Eq. (2-11). The effective elastic modulus takes into account the fact that elastic displacements occur in both the specimen, with Young's modulus E and Poisson's ratio ν, and the indenter, with elastic constants E_i and ν_i. Note that Eq. (2-35) is a very general relation that applies to any axisymmetric indenter [64,65]. It is not limited to a specific simple geometry, even though it is often associated flat punch indentation. Although originally derived for elastic contact only [64], it has subsequently been shown to apply equally well to elastic-plastic contact [65], and that small perturbations from pure axisymmetry geometry do not effect it either [66]. It is also unaffected by pile-up and sink-in.

- **Residual Stress**

Indentation hardness as analyzed from the indentation *P-h* curve changes with the material residual stress: indentation *P-h* curves are shifted with the direction and magnitude of residual stress within the tested material. However, the variations in the apparent indentation hardness with change in residual stress have been identified as an artifact of erroneous optical measurements of the indentation imprint [67]: in a study of the influence of in-plane stress on indentation plasticity that investigated both the

shape of the indentation curve and the contact impressions, the contact hardness was found to be invariant regardless of the elastically applied stress (residual stress) [67]. The FEA results showed the important role of sink-in or pile-up deformations around the contact in the stressed state in producing the stress-insensitive contact hardness. Therefore, the change in contact morphologies with residual stress was modeled for constant maximum indentation depth assuming the independence of intrinsic hardness and residual stress [68].

The change in indentation deformation caused by the residual stress was identified in the indentation loading curve in Fig. 2.9. The applied load in the tensile-stressed state is lower than that in the stress-free state for the same maximum indentation depth [67,68]. In other words, the maximum indentation depth desired is reached at a smaller indentation load in a tensile-stressed state because a residual-stress-induced normal load acts as an additive load to the applied load. Therefore, the residual stress can be evaluated by analyzing the residual-stress-induced normal load.

The detailed changes in contact morphology can be seen in the schematic diagram in Fig. 2.10. The residual stress is relaxed from a tensile-stressed state to stress-free state while maintaining the constant maximum depth, h_{max}, as the stress relaxation pushes the indenter out from the surface. The

pushing force appears as an increase in the applied load ($L_T \rightarrow L_0$) and the contact depth ($h_c^T \rightarrow h_c$), because the maximum depth is held constant. The indentation load and maximum depth for the tensile-stressed state (L_T, h_{max}) are equivalent to those in the relaxed state (L_0, h_{max}). Thus, the relationship between the two states can be expressed as

$$L_0 = L_T + L_{res} . \tag{2-36}$$

In the compressive stress state, the applied load and contact depth decrease by stress relaxation under the maximum-depth-controlled path. Furthermore, this decreasing portion of the applied load was the residual-stress-induced normal load, L_{res}. Therefore, the residual stress in a welded joint can be evaluated by dividing L_{res} by the contact area, A_c, regardless of the stress state [69]

$$\sigma_{res} = \alpha \frac{L_{res}}{A_c}, \tag{2-37}$$

where α is a constant related to the stress directionality of biaxial residual stress. The biaxial stress state, in which $\sigma_y = k\sigma_x$, can be divided into a mean stress term and plastic-deformation-sensitive shear deviator term [69]

Biaxial stress *Mean stress* *Deviator stress*

$$\begin{pmatrix} \sigma^{x}_{res} & 0 & 0 \\ 0 & \sigma^{y}_{res} & 0 \\ 0 & 0 & 0 \end{pmatrix} = \begin{pmatrix} \frac{1+k}{3}\sigma^{x}_{res} & 0 & 0 \\ 0 & \frac{1+k}{3}\sigma^{x}_{res} & 0 \\ 0 & 0 & \frac{1+k}{3}\sigma^{x}_{res} \end{pmatrix} + \begin{pmatrix} \frac{2-k}{3}\sigma^{x}_{res} & 0 & 0 \\ 0 & \frac{2-k}{3}\sigma^{x}_{res} & 0 \\ 0 & 0 & -\frac{1+k}{3}\sigma^{x}_{res} \end{pmatrix}$$

. (2-38)

The stress component parallel to the indentation axis in the deviator stress term directly affects the indenting plastic deformation. A residual-stress-induced normal load L_{res} can be defined from the selected deviator stress component as

$$L_{res} = \frac{1+k}{3}\sigma_{res}A_c . \tag{2-39}$$

Therefore, α in Eq. (2-37) can be taken as approximately 1.5 in the equi-biaxial stress state. In the instrumented indentation test, the contact area is determined by unloading curve analysis. By differentiation of the power-law-fitted unloading curve at maximum indentation depth, the contact depth and contact area can be calculated from the contact depth based on the geometry of the Vickers indenter as [84]

$$A_c = 24.5h_c^{2} . \tag{2-40}$$

Thus, residual stress was calculated from the analyzed contact

area in Eq. (2-39) and the measured load change L_{res} by the effect of residual stress in Eq. (2-36).

- **Fracture Toughness**

Indentation fracture toughness is a simple technique for determination of fracture toughness [70-77]. The indentation cracking method is especially useful for measurement of fracture toughness of thin films or small volumes. This method is quite different from conventional methods in that no special specimen geometry is required. Rather, as shown schematically in Fig. 2.11, these techniques make use of the radial cracking that occurs when brittle materials are indented by a sharp indenter such as a Vickers or Berkovich indenter [71]. Based on fracture mechanics analysis, Lawn *et al.* [71] have shown that a simple relationship exists between the fracture toughness (K_c) and the lengths of the radial cracks (c) of the form

$$K_c = \alpha\left(\frac{E}{H}\right)^{1/2}\left(\frac{P_{\max}}{c^{3/2}}\right) \tag{2-41}$$

where α is an empirical constant dependent on the geometry of the indenter. It was found that the value of 0.016 could give good correlation between the toughness values measured from the crack length and the

ones obtained using more conventional methods [78]. An attractive feature of using this method in nanoindentation is that both H and E can be determined directly from analyses of nanoindentation force-depth data. Thus, provided one has a way to measure crack lengths, implementing the method is relatively straightforward.

- **Tensile Properties**

Knapp *et al.* [79,80] tried to determine the yield strength and elastic modulus for amorphous or nonmetallic materials, in which work hardening can be assumed to be zero. By limiting the material parameters to be varied to yield strength Y and elastic modulus E (two unknown parameters), Y and E were fitted to linear functions of the force F and stiffness S at a particular depth (two known parameters):

$$Y = a_1 S + b_1 F + c_1 \qquad (2\text{-}42)$$

$$E = a_2 S + b_2 F + c_2 \qquad (2\text{-}43)$$

To determine the coefficients of Eq. (2-42) and (2-43), a series of FEM simulations were performed with different trial values of Y and E (Fig. 2.12(a)). Fig. 2.12(b) shows the values of force and stiffness calculated from the material properties in Fig. 2.12(a). Thus, the interpolation of the

best Y and E to S and F can be accomplished by a three-parameter linear interpolation function. Y and E for $Fe_{64}Ti_{18}C_{18}$ (solid diamond in Fig. 2.12(a)) were extrapolated from the experimental F and S (solid square in Fig. 2.12(b)) by the above interpolation function.

For geometrically similar indenters, the average plastic strain beneath an indenter is represented as representative plastic strain (ε_R), which is calculated from the strain definition in terms of indentation geometry. The representative plastic strain should be such that it is dependent on the geometry of the self-similar indenter and independent of penetration depth [81].

On the other hand, at large indentation depths, i.e., in the full plastic-flow regime, Tabor [2] suggested the following relationship to estimate flow stress (σ_R) from hardness values (H):

$$H = C\sigma_R \qquad (2\text{-}44)$$

where C is constant and σ_R is a flow stress corresponding to the ε_R. Therefore, with at least two different tip shapes, two points on the stress-strain curve at higher strains can be estimated and used to extrapolate the stress-strain curves. Fig. 2.13(a) shows schematically the determination of stress-strain curve from cone indentation testing with various apical

angles.

Jayaraman *et al.* [81] obtained a stress-strain curve for Si_3N_4 (Fig. 2.13(b)) by calculating representative plastic strain values for indenters having different angles (0.07 for a cone with a half-angle of 70.3° and 0.225 for 42.3°). The flow stress values corresponding to these representative strains were determined from the experimental hardness values.

A scaling approach is based on dimensional analysis, which is a mathematical tool for simplifying a problem by reducing the number of variables to the smallest number of essential parameters. For a sharp indenter, the indentation force (F) can be written as

$$F = F(d, E_r, \sigma_y, n) \qquad \text{(2-45a)}$$

or

$$F = F(d, E_r, \sigma_R, n) \qquad \text{(2-45b)}$$

where d is indentation depth, E_r is the reduced modulus, n is the strain-hardening exponent, and σ_R is the representative stress defined at ε_R.

By applying the Π theorem in dimensional analysis, Eq. (2-45b) becomes

$$\frac{F}{d^2} = \sigma_R \prod\left(\frac{E_r}{\sigma_R}, n\right) \qquad \text{(2-46)}$$

The function Π in Eq. (2-46) has only two essential parameters, while Eq. (2-45) has four. The specific functional form of Π depends on the choice of ε_R and σ_R. Suresh *et al.* [86] found a representative plastic strain value of 0.033 at which Π is independent of the strain-hardening exponent (n) (Fig. 2.14). Π can relate σ_R to the measured F/d^2 when E_r is known. Other universal dimensionless functions can be also constructed to relate the indentation response (unloading slope, work done during loading, maximum and residual indentation depth, etc.) to mechanical properties (E_r, σ_y, σ_R, n, etc.).

Table 2.1

Projected areas, intercept corrections, and geometry correction factors for various types of indenters. The semi-angles given for pyramidal indenters are the face angles with the central axis of the indenter.

Indenter type	Projected area, A	Semi-angle, (degree)	Effective cone angle, (degree)	Intercept factor	Geometry correction factor,
Sphere	$2\pi R h_c$	N/A	N/A	0.75	1
Berkovich	$3\sqrt{3}\tan^2\theta \cdot h_c^2$	65.3	70.2996	0.75	1.034
Vickers	$4\tan^2\theta \cdot h_c^2$	68	70.32	0.75	1.012
Knoop	$2\tan\theta_1 \tan\theta_2 \cdot h_c^2$	$_1$=86.25 , $_2$=65	77.64	0.75	1.012
Cube corner	$3\sqrt{3}\tan^2\theta \cdot h_c^2$	35.26	42.28	0.75	1.034
Cone	$\pi\tan^2\alpha \cdot h_c^2$			0.72	1

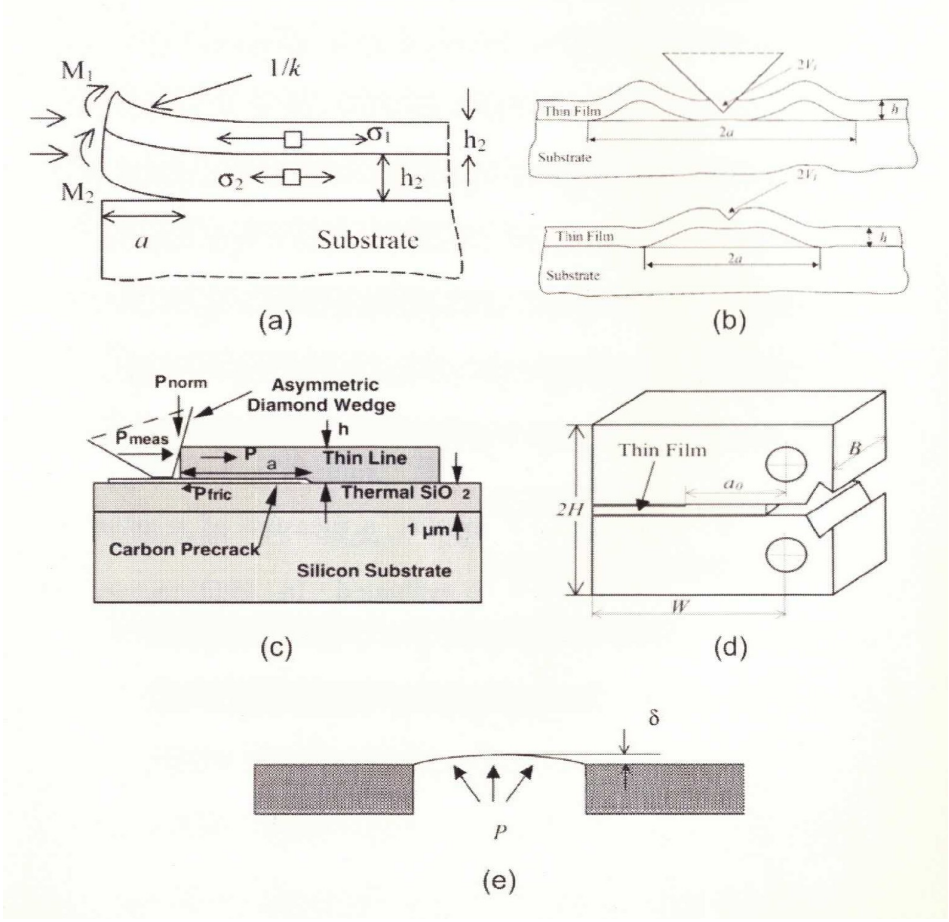

Figure 2.1. Schematic diagram of (a) super-layer test, (b) indentation test, (c) scratch test, (d) sandwich specimen test, and (e) bulge and blister test.

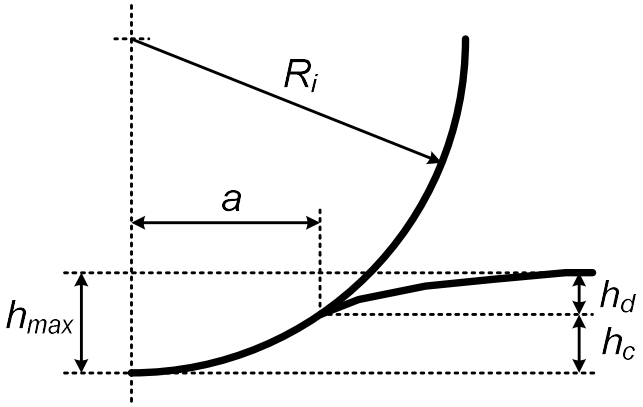

Figure 2.2. Schematic of contact between rigid indenter and flat specimen with Young's modulus E. a is radius of circle of contact, h_{max} is total depth of penetration, h_d is depth of circle of contact from specimen free surface, and h_c is the distance from bottom of contact to contact circle.

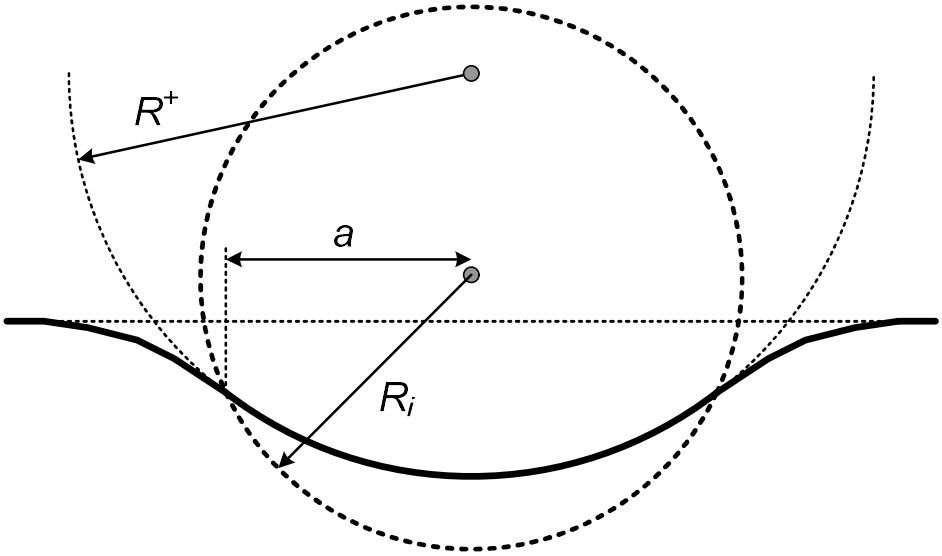

Figure 2.3. Contact between non-rigid indenter and flat surface of specimen with Young's modulus *E*.

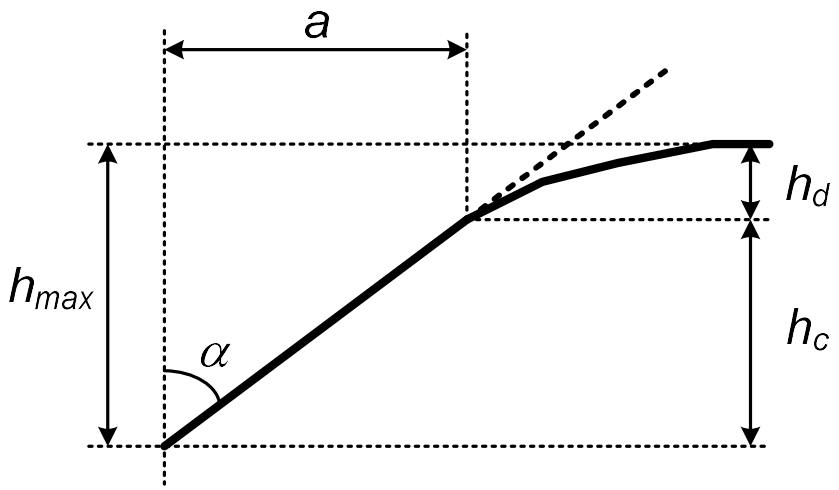

Figure 2.4. Geometry of contact with conical indenter.

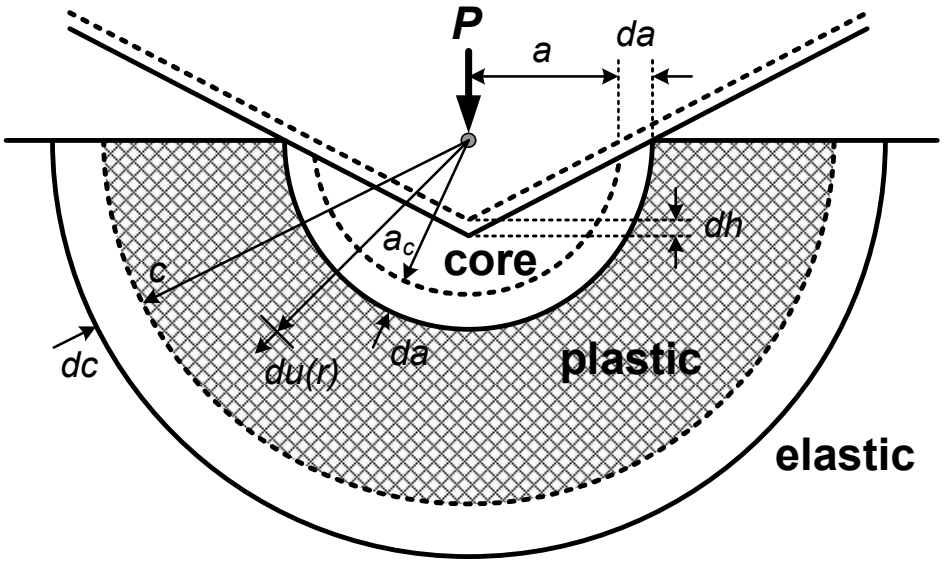

Figure 2.5. Schematic of expanding cavity model.

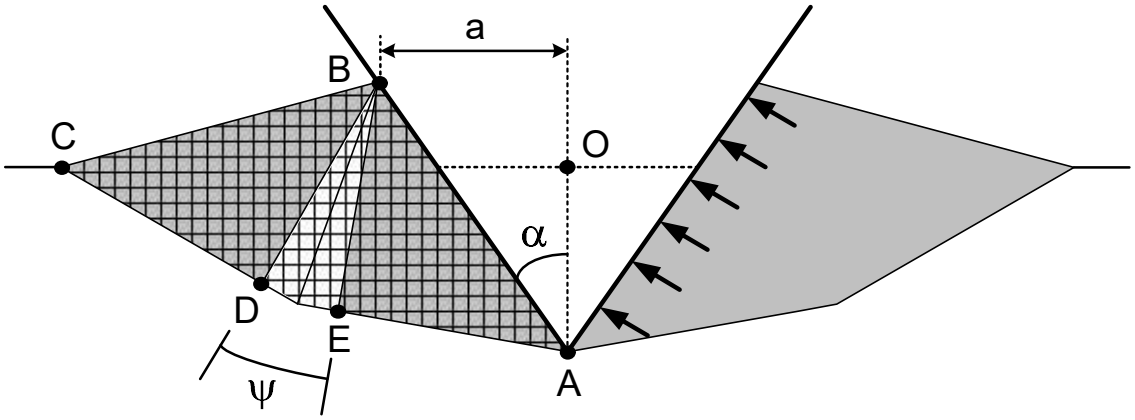

Figure 2.6. Slip-line theory.

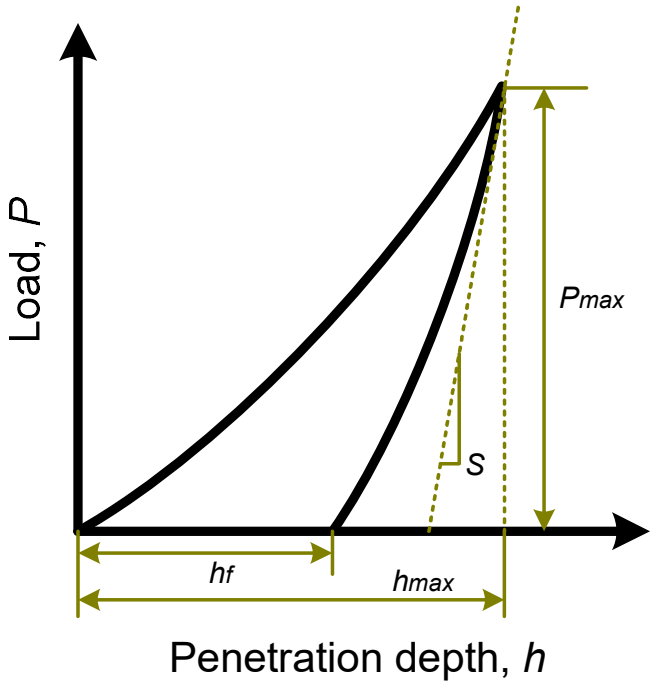

Figure 2.7. Schematic of indentation load-depth curve.

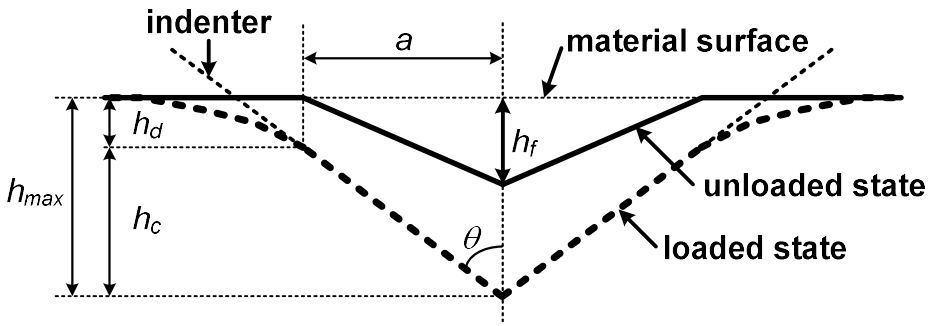

Figure 2.8. Cross section of contact morphology in loaded state and residual indent after unloading by sharp indenter.

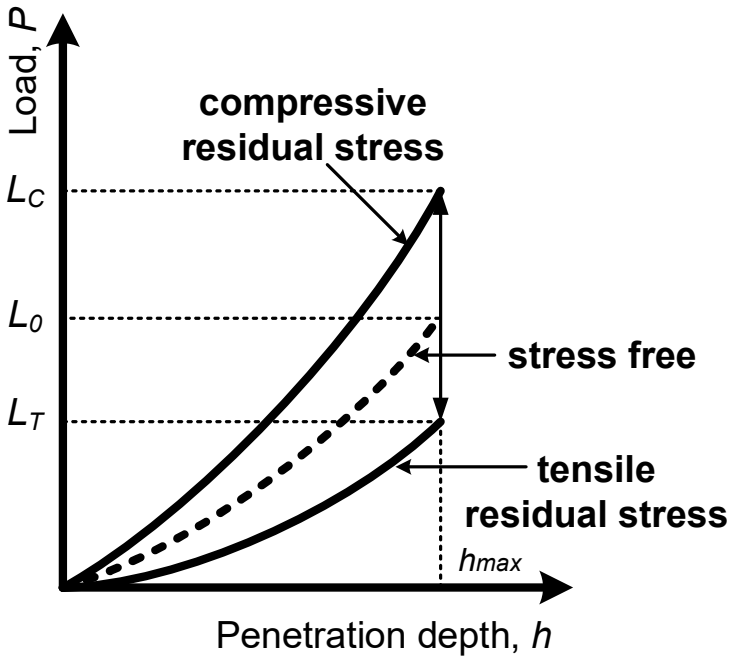

Figure 2.9. Variation of indentation loading curves with changes in the stress state.

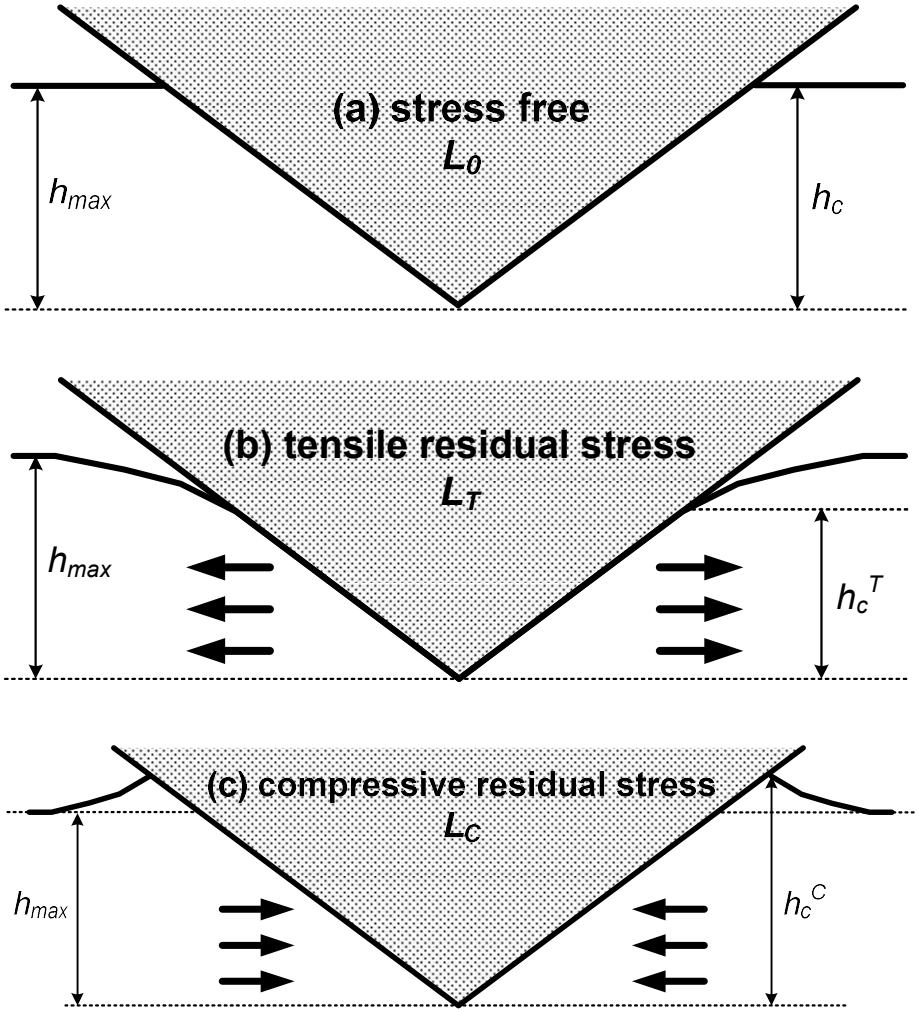

Figure 2.10. Theoretical surface morphologies around the indenter for (a) stress-free, (b) tensile stress, and (c) compressive stress states.

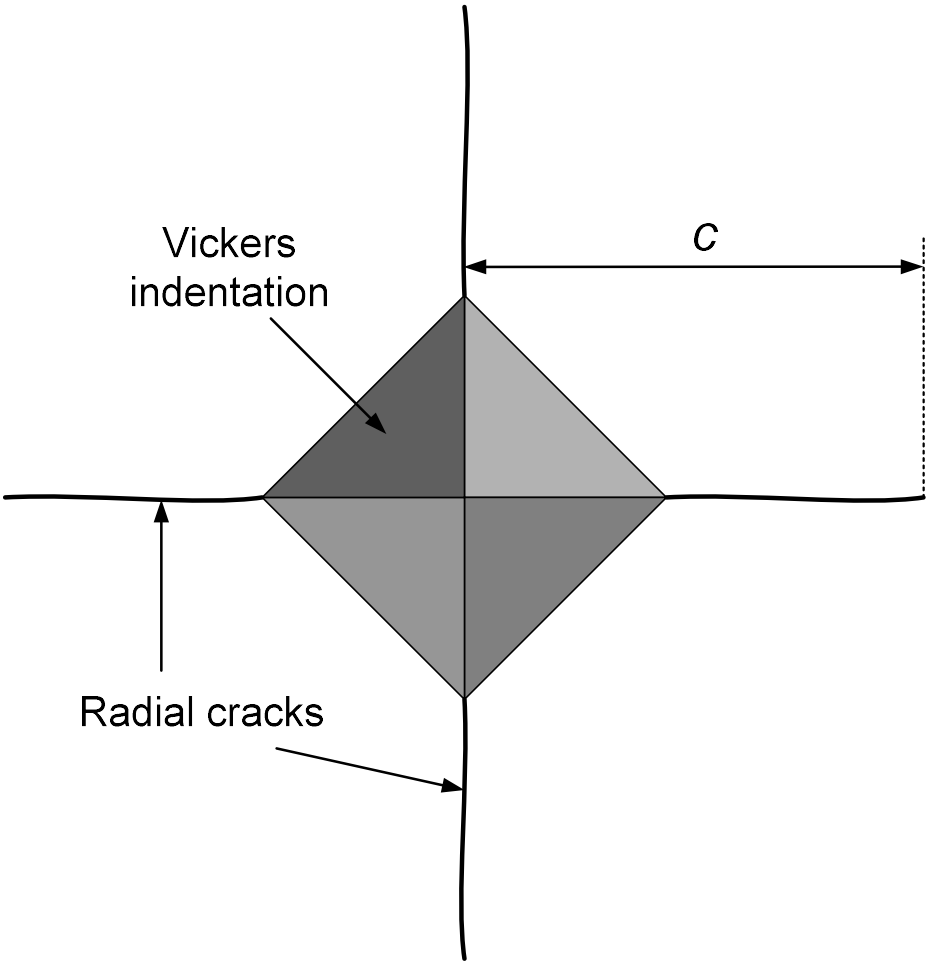

Figure 2.11. Schematic of radial cracking by Vickers indentation.

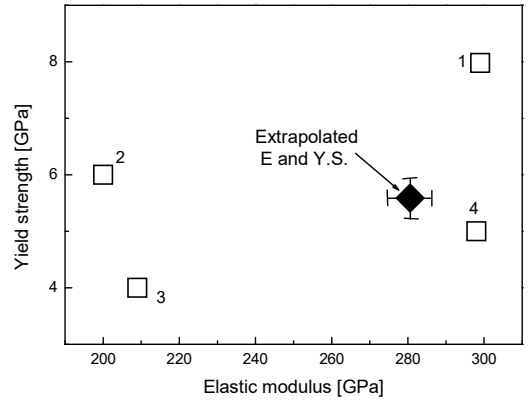

(a)

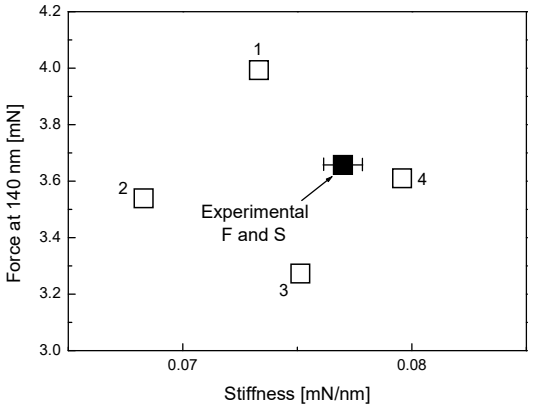

(b)

Figure 2.12. (a) Trial values of *Y* and *E* for $Fe_{64}Ti_{18}C_{18}$ layer (open squares); the solid diamond represents the final interpolated *Y*, *E* pair. (b) Corresponding values of force and stiffness resulting from simulations using (a); the solid square is average force and stiffness from the experimental data.

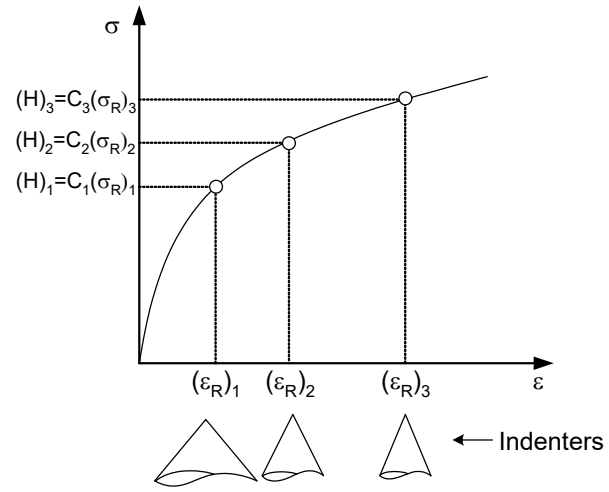

(a)

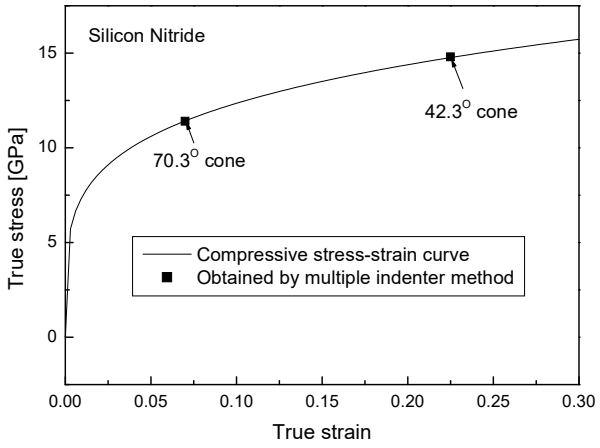

(b)

Figure 2.13. (a) Schematic for obtaining stress-strain values using cone indentation with various apical angles and (b) stress-strain curve of silicon nitride calculated from cone indentation tests with various apical angles.

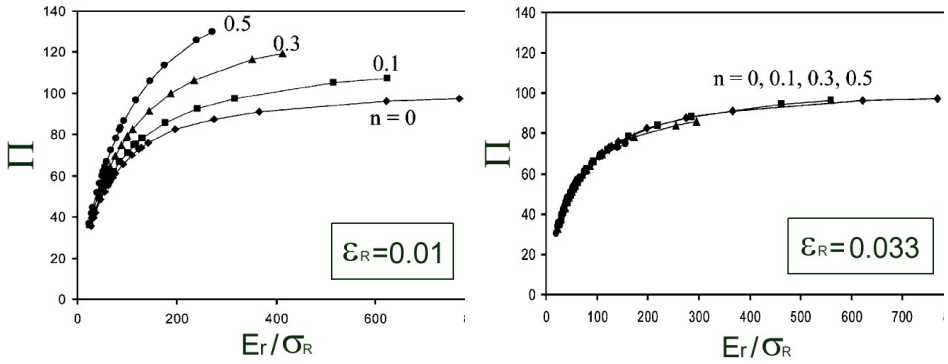

(a) (b)

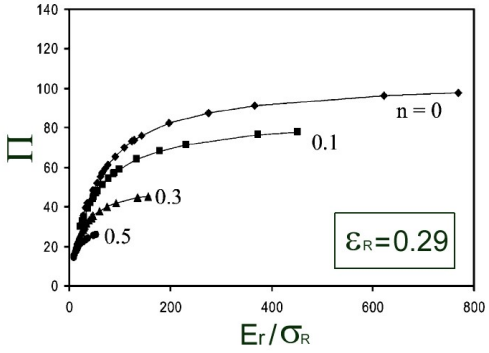

(c)

Figure 2.14. Dimensionless function Π relating F/d^2 to representative stress corresponding to various representative plastic values: (a) ε_R=0.01, (b) ε_R =0.033, and (c) ε_R =0.29. The representative plastic strain ε_R =0.033 can be identified as the strain value that allows the construction of Π to be independent of the strain-hardening exponent, *n*.

Chapter 3

THEORETICAL MODELING

Contents

3.1. Thin-film indentation

Determination of the mechanical properties of thin films on substrates by indentation has always been difficult because of the influence of the substrate and interface on the measured properties[13]. In order to measure ‘film-only’ properties, a commonly used rule of thumb is to limit the indentation depth to less than 10% of the film thickness.

As the film gets harder, the substrates and interfacial effects appear at lower indentation depth. Many researchers derived the conclusion from the theoretical and experimental methods[2,3,4,5]. In the case of thin films which have thickness under than from nanometers to micrometers, it has no choice but must include the substrates and interfacial effects. Owing to the quantitative consideration about interfacial effects was hard, modeling equations with no interfacial effects is used. The amount of work got from the indentation test with no interfacial effects can be expressed as:

$$W_{total} = W_{film} + W_{substrate} \tag{3-1}$$

where W_{total} is the total amount of work, W_{film} is the amount of work done by film and $W_{substrate}$ is the amount of work done by substrate. To

distinguish each of the amount of work, FEM analysis [87-89] interpreting elastic-plastic deformation and idealized geometrical approach are used after an experimental approach is proposed. But in the real indentation tests, there are not only the effects from substrate but also interfacial work exists. Namely, the total work done at depth more than 10% in indentation tests is sum of the amount of work done by film, substrate and the work done by the interface.

$$W_{total} = W_{film} + W_{substrate} + W_{adhesion} \quad (3\text{-}2)$$

In here, the friction force between indenter tip and film surface is not considered. $W_{adhesion}$ is virtual value which means a work done by interface. Because it is impossible to distinguish each of the film, substrate and interfacial work experimentally, theoretical modeling to develop formulae is used.

3.2. Interfacial Constraint Effect

During indentation, a stress field develops inside the specimen under the indenter. Many researchers have used an expanding cavity model (ECM) to describe the stress field during indentation because of its simplicity and predictability. Hill suggested a solution for the quasi-static expansion of an internally pressurized spherical shell of an elastic-perfectly plastic material [35]. In Johnson's ECM [33], a hemispherical hydrostatic core is assumed to be located around the indenter. For conical indentations, he predicted an ECM based on the von Mises and material incompressibility assumptions as:

$$\frac{H}{\sigma_y} = \frac{2}{3}\left[1 + \ln\left(\frac{1}{3}\frac{E}{\sigma_y}\cot\alpha\right)\right] \tag{3-3}$$

where H, σ_y, and E are the hardness, yield strength and elastic modulus of specimen, respectively, and α is the semi-included angle of a conical indenter. However, since Johnson's ECM was not appropriate for characterizing indentation deformations of strain-hardening materials [90, 91], finite element simulations have been used to study indentation deformations of strain-hardening materials with a sharp indenter [92-95] or spherical indenter [96-98]. Gao et al. [99], to overcome this limitation, suggested a new expanding cavity model considering constitutive

equation for hardening behavior:

$$\frac{H}{\sigma_y}=\frac{2}{3}\left[\left(1-\frac{1}{n}\right)+\left(\frac{3}{4}+\frac{1}{n}\right)\left(\frac{1}{3}\frac{E}{\sigma_y}\cot\alpha\right)^{n}\right] \tag{3-4}$$

$$\frac{H}{\sigma_y}=\frac{2}{3}\left[\frac{7}{4}+\frac{7}{4}\frac{E_p}{E}\left(\frac{1}{3}\frac{E}{\sigma_y}\cot\alpha-1\right)+\left(1-\frac{E_p}{E}\right)\ln\left(\frac{1}{3}\frac{E}{\sigma_y}\cot\alpha\right)\right] \tag{3-5}$$

Eqs. (3-4) and (3-5) are the modified formulas for power-law hardening and linear-hardening materials, respectively.

According to Gao's model as shown in Fig. 4.6, the plastic zone radius *c* for a conical indenter can be expressed as:

$$\left(\frac{c}{a}\right)^{3}=\frac{1}{3}\frac{E}{\sigma_y}\cot\alpha \tag{3-6}$$

where *a* is the contact radius of conical indentation.

H. Li, Jeong-Hoon Ahn proposed that, increasing the indentation depth, the expanding plastic zone is constraint by interface. According to the research, in the thin film/substrate system, the relatively soft materials are constrained by relatively hard materials. When the thin film is relatively hard and substrate is soft, the plastic zone volume in the substrate is constrained by the interface, and when the thin film is relatively soft and substrate is hard, the plastic zone volume size in the

thin film is constrained by the interface. In other words, the constraint materials are determined from the hardness ratio of the thin films and substrates.

The condition which films are constrained is expressed as:

$$\frac{H_s}{H_f} > 1 \tag{3-7}$$

And the condition which substrates are constrained is expressed as:

$$\frac{H_s}{H_f} < 1 \tag{3-8}$$

where subscript ***f*** is film and ***s*** is substrate.

The plastic zone radius(C) determined by the ratio of elastic modulus E to hardness H has 2 different case to find in thin film/substrate system. First, the plastic zone radios of thin films is greater than that of the substrates because the E/H ratio of the thin films is greater than that of the substrates. Second, the plastic zone radio of substrates is greater than that of the thin films because the E/H ratio of the substrates is greater than that of the thin films.

The condition which the plastic zone radius of thin films is greater than that of the substrates is expressed as:

$$\left(\frac{E}{H}\right)_f > \left(\frac{E}{H}\right)_s \tag{3-9}$$

The condition which the plastic zone radius of substrates is greater than that of the thin films is expressed as:

$$\left(\frac{E}{H}\right)_f < \left(\frac{E}{H}\right)_s \tag{3-10}$$

The constrained materials are determined by hardness ratio and the constrained directions are determined by the elastic modulus/hardness ratio. There are 4 situations beneath of the indenters considering constrained materials and directions. It is shown in Fig. 3.1.

I. $H_f < H_s$, $\left(\frac{E}{H}\right)_f < \left(\frac{E}{H}\right)_s$: Film positive constraint

II. $H_f < H_s$, $\left(\frac{E}{H}\right)_f > \left(\frac{E}{H}\right)_s$: Film negative constraint

III. $H_f > H_s$, $\left(\frac{E}{H}\right)_f > \left(\frac{E}{H}\right)_s$: Substrate positive constraint

IV. $H_f > H_s$, $\left(\frac{E}{H}\right)_f < \left(\frac{E}{H}\right)_s$: Substrate negative constraint

Positive constraint means that the constraint is done to the volume

increasing direction while negative means that the constraint is done to the volume decreasing direction. Following the adhesion strength, the constraining force becomes different and constraint volume changes too. The relatively better adhesion makes increased constraint volume with decreased interfacial slips. In the opposite case, the constraint volume decreases with increased interfacial slips. It is shown in Fig. 3.2.

3.3. Interface parameter

The interface parameter (χ^3) is proposed to express constraint volume of relatively soft materials. The parameter of χ^3 shows plastic volume changes by interface effectively [13].

Interface parameter can be expressed with the ratio of the volume before constraint to the volume after constraint as:

$$\chi^3 = \frac{V^*}{V} \tag{3-11}$$

where V^* is plastic volume before constraint and V is plastic volume after constraint. In the case of positive film/substrate constraint which the volume expands by the constraining effect, the interface parameter has the value higher than 1. In the opposite case the negative film/substrate constraint which the volume reduces by the constraining effect, the interface parameter has the value between 0 and 1.

Through this interface parameter, the constraint volume change is modeled.

When the thin films are constrained, the plastic volume before constraint is expressed as :

$$V_{total} = V_f + V_s \tag{3-12}$$

and the plastic volume after constraint is expressed as:

$$V_{total}^{*} = V_{f}^{*} + V \tag{3-13}$$

where V_f^* is $V_f \cdot \chi^3$.

When the substrates are constrained, the plastic volume before constraint is expressed as:

$$V_{total} = V_f + V_s \tag{3-15}$$

and the plastic volume after constraint is expressed as:

$$V_{total}^{*} = V_f + V_s^{*} \tag{3-16}$$

where V_s^* is $V_s \cdot \chi^3$.

It is modeled to derive interface parameter quantitatively.

N. A. Stillwell, D. Tabor proposed that the concept of hardness conventionally defined as the force over area can be expanded as the work of indentation over deforming volume[48]. T. F. Page explained the hardness has the equivalent value with the ratio of plastic work to plastic deforming volume.

$$H = \frac{W_{plastic\ work\ of\ indentation}}{V_{plastic\ deforming\ volume}} \tag{3-17}$$

When substitute the equation(3-17) to the equation(3-2) and make it up

with the modified volume in the equation(3-13), the interface parameter when the thin films are constrained is obtained.

$$\chi^3 = \frac{V_s(H_s - H_c)}{V_f(H_c - H_f)} \tag{3-18}$$

Likewise, substitute the equation(3-17) to the equation(3-2) and make it up with modified volume in the equation(3-16), the interface parameter when the substrates are constrained is obtained.

$$\chi^3 = \frac{V_f(H_f - H_c)}{V_s(H_c - H_s)} \tag{3-19}$$

The interface parameter consists of H_f, H_s, V_f, V_s with no interfacial effect and H_c with interfacial effects. Using this equation, the interface parameter can be obtained experimentally.

3.4. Factor analysis

When operating indentation tests, the expanding plastic volume is constrained by the interface. In the case of negative constraint, plastic volume reduces and the opposite, positive constraint, plastic volume expands.

I. Negative constraint

Negative constraint gets limitation on the deformation of expansion by adhesion strength. It causes compressive stress in the relatively soft material. It is shown in Fig. 3.3. Compressive stress occurred in material enhances load measured at the same indentation depth. As it gets advanced adhesion, greater plastic volume is constrained, resulting higher compressive stress state. Then the measured load gets higher at the same indentation depth as it has better adhesion. It is shown in Fig. 3.4.

II. Positive constraint

Positive constraint gets limitation on the deformation of reduction by adhesion strength. It causes tensile stress in the relatively soft material. It is shown in Fig. 3.5. Tensile stress occurred in material lowers load

measured at the same indentation depth. As it gets better adhesion, greater plastic volume is constrained, resulting higher tensile stress state. Then the measured load gets lower at the same indentation depth as it has better adhesion. It is shown in Fig. 3.6.

3.5. Modeling

Work of adhesion can be calculated from the difference of the equation (3-1) and (3-2) as:

$$W_{total}^{*} - W_{total} = W_{adhesion} \tag{3-20}$$

where W_{total}^{*} is work regarding the effect of the interface, while W_{total} is from the ideal situation with no effect of the interface.

With equation(3-20), equation(3-17) can be expressed as eq.(3-21) and eq.(3-22)

$$W_{total} = H_f \cdot V_f + H_s \cdot V_s \tag{3-21}$$

$$W_{total}^{*} = H_f \cdot V_f + H_s \cdot V_s + W_{adheion} \tag{3-22}$$

3.5.1. Film constraint model

Plastic volume constraint by interfacial effect is explained at chapter 3.3. Using dimensionless interface parameter χ^3, eq. (3-13) shows the degree of constraining.

Substituting in eq. (3-13) to eq. (3-22) can expressed as:

$$W_{total}^{*} = V_f \cdot H_f + V_s \cdot \chi^3 \cdot H_s \tag{3-23}$$

In here, eq. (3-24) is obtained with substituting eq. (3-18) for eq. (3-21)

$$W_{total}^{*} = V_f \cdot H_f + V_s \cdot [\frac{V_s(H_s - H_c)}{V_f(H_c - H_f)}] \cdot H_s \tag{3-24}$$

Work of adhesion can be derived by substituting eq. (3-24) and eq. (3-21) for eq. (3-20).

$$W_{adhesion} = \left[V_f \cdot H_f + V_s \cdot [\frac{V_s(H_s - H_c)}{V_f(H_c - H_f)}] \cdot H_s \right] - \left[H_f \cdot V_f + H_s \cdot V \right] \tag{3-25}$$

Eq. (3-25) can expressed as:

$$W_{adhesion} = H_f \cdot V_f(\chi^3 - 1) \tag{3-26}$$

3.5.2. Substrate constraint model

Plastic volume constraint by interfacial effect is explained at chapter 3.3. Using dimensionless interface parameter χ^3, eq. (3-16) shows the plastic volume after constraint.

Now substituting eq. (3-16) for eq. (3-22) can expressed as:

$$W_{total}^{*} = V_f \cdot \chi^3 \cdot H_f + V_s \cdot H_s \quad (3\text{-}27)$$

In here, eq. (3-28) is obtained with substituting eq. (3-19) for eq. (3-21)

$$W_{total}^{*} = V_f \cdot H_f + V_s \cdot [\frac{V_s(H_s - H_c)}{V_f(H_c - H_f)}] \cdot H_s \quad (3\text{-}28)$$

Work of adhesion can be derived by substituting eq. (3-28) and eq. (3-21) for eq. (3-20).

$$W_{adhesion} = \left[V_f \cdot H_f + V_s \cdot [\frac{V_f(H_f - H_c)}{V_s(H_c - H_s)}] \cdot H_s \right] - \left[H_f \cdot V_f + H_s \cdot V \right] \quad (3\text{-}29)$$

Eq. (3-29) can expressed as:

$$W_{adhesion} = H_s \cdot V_s(\chi^3 - 1) \quad (3\text{-}30)$$

It was derived considering of interfacial constraint effect, composite hardness based 'film constraint work of adhesion model"(eq. 3-26) and "substrate constraint work of adhesion model""(eq. 3-30)

Calculated work of adhesion through modelling increases as the indentation depth increases like (Fig. 3.7). Because the area effect by interface becomes larger as the indentation depth increases. The plastic zone radius increases one-dimensionally depending on the eq. (3-6). Likewise, constraint deforming volume effected by interface increases three-dimensionally. To derive quantitative work of adhesion regardless of the condition of test, normalization is needed. It is the work done to constrain plastic volume that eq. (3-26) and eq. (3-30) through the modeling. Therefore, quantitative value is derived from normalizing plastic volume before constraint. Film constraint model is normalized with V_f and substrate constraint model is normalized with V_s. Finally, adhesion strength is derived from normalizing with the volume before constraint.

I. Film constraint model

$$\sigma_{adhesion} = H_f(\chi^3 - 1) \tag{3-31}$$

II. Substrate constraint model

$$\sigma_{adhesion} = H_s(\chi^3 - 1) \tag{3-32}$$

3.6. Physical meaning of equation

The relationship of derived final equation and physical meaning are considered.

I. Film constraint model

A. Positive constraint (Expansion of deforming volume)

: In better adhesion, plastic deformation volume increases more easily causing higher tensile stress state in the thin film. Higher tensile stress state makes lower maximum load at same indentation depth. Composite hardness gets smaller as load decreases and in this case, interface parameter is bigger than 1. It means that the plastic deformation volume increasing by the interfacial effect. When the interface parameter gets bigger, adhesion strength also increases according to eq. (3-31) (Fig. 3.8)

B. Negative constraint (Reduction of deforming volume)

: In better adhesion, plastic deformation volume increasing gets more difficult causing higher compressive stress state in the thin film. Higher compressive stress state makes higher maximum load at the same indentation depth. Composite hardness gets bigger as load increases and in this case, interface parameter is smaller than 1. It means that the plastic

deformation volume decreasing by the interfacial effect. When the interface parameter gets smaller, adhesion strength increases according to eq. (3-31). Because adhesion strength has negative value in the case of negative constraint, the magnitude is obtained with its absolute value.

In the case of films constraint shown in Fig. 3.8.

II. Substrate constraint model

A. Positive constraint (Expansion of deforming volume)

: In better adhesion, plastic deformation volume increases more easily causing higher tensile stress state in the substrate. Higher tensile stress state makes lower maximum load at same indentation depth. Composite hardness gets smaller as load decreases and in this case, interface parameter is bigger than 1. It means that the plastic deformation volume increasing by the interfacial effect. When the interface parameter gets bigger, adhesion strength also increases according to eq. (3-32)

B. Negative constraint (Reduction of deforming volume)

: In better adhesion, plastic deformation volume increasing gets more difficult causing higher compressive stress state in the substrate. Higher compressive stress state makes higher maximum load at the same

indentation depth. Composite hardness gets bigger as load increases and in this case, interface parameter is smaller than 1. It means that the plastic deformation volume decreasing by the interfacial effect. When the interface parameter gets smaller, adhesion strength increases according to eq. (3-32). Because adhesion strength has negative value in the case of negative constraint, the magnitude is obtained with its absolute value. In the case of substrate constraint shown in Fig. 3.9. Fig. 3.10 showed a schematic diagram of relation of indentation phenomena and indentation parameter by indentation test.

	$H_f > H_s$ (Sub. Constraint)	$H_f < H_s$ (Film Constraint)
$C_f > C_s$	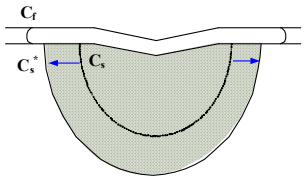 **Positive constraint** (= **Expansion** of substrate plastic volume)	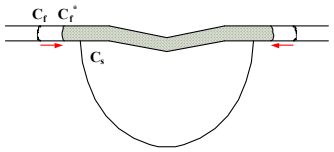 **Negative constraint** (=**Reduction** of film plastic volume)
$C_f < C_s$	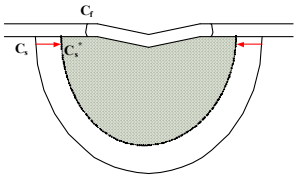 **Negative constraint** (= **Reduction** of substrate plastic volume)	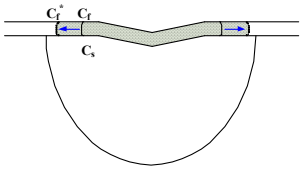 **Positive constraint** (= **Expansion** of film plastic volume)

Figure 3.1. 4 kinds of situation beneath indenter

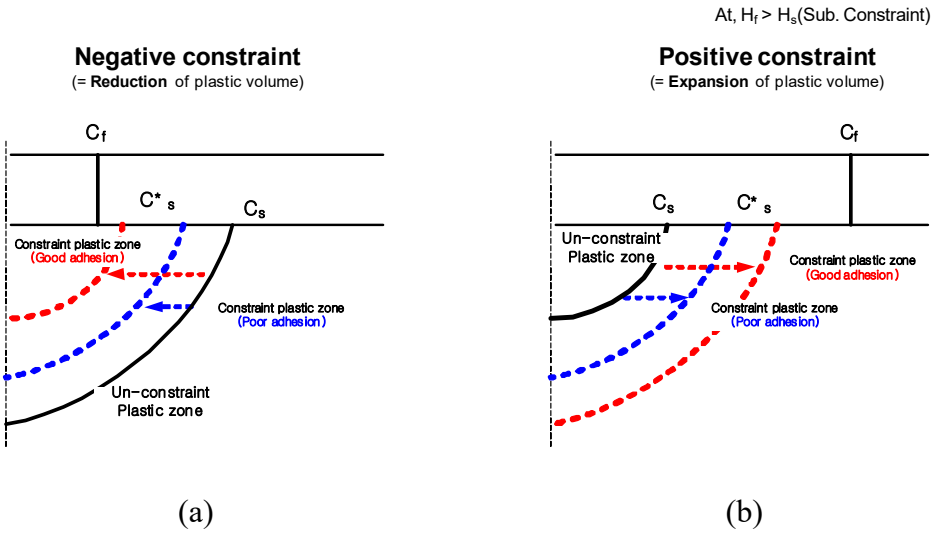

Figure 3.2. Schematic diagram for

(a) negative constraint volume change and (b) positive constraint volume change

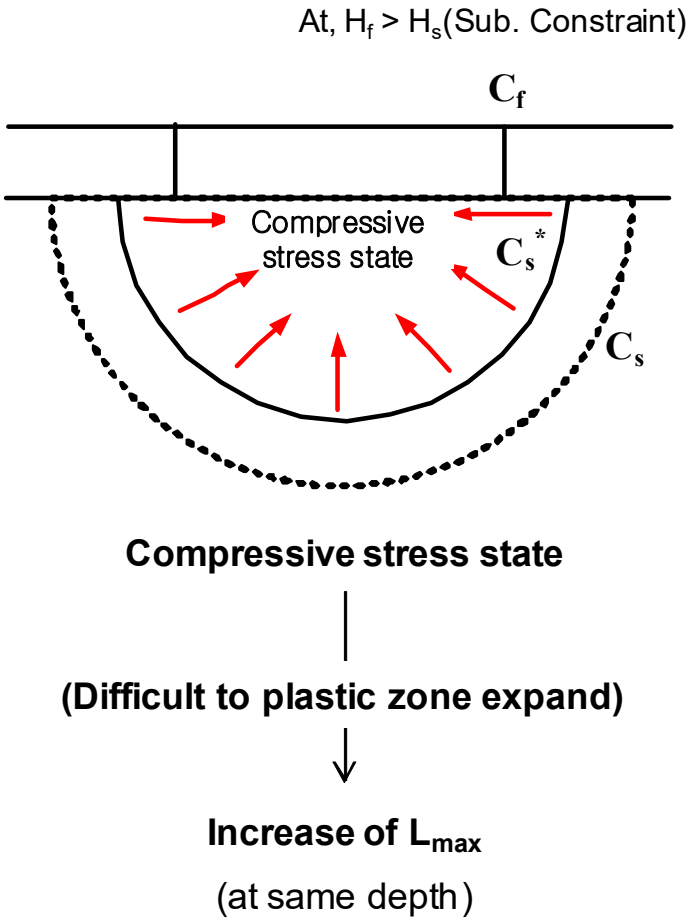

Figure 3.3. Load differences due to the interface at negative constraint

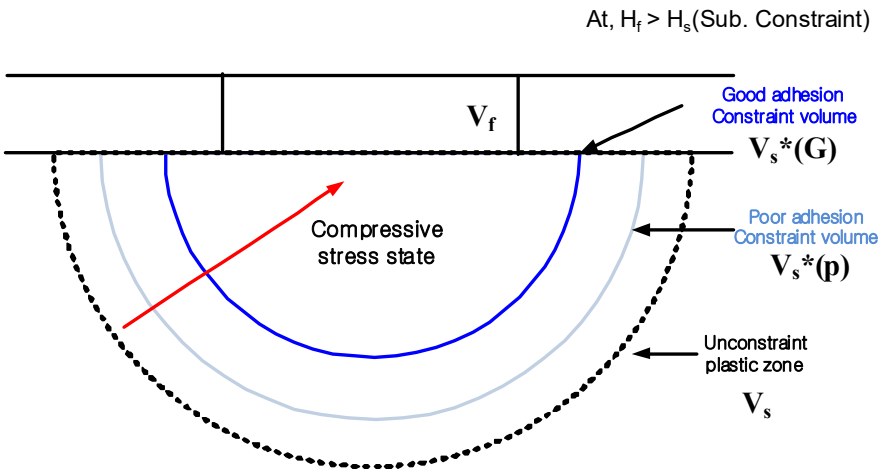

Figure 3.4. Change in volume difference according to adhesion at negative constraint

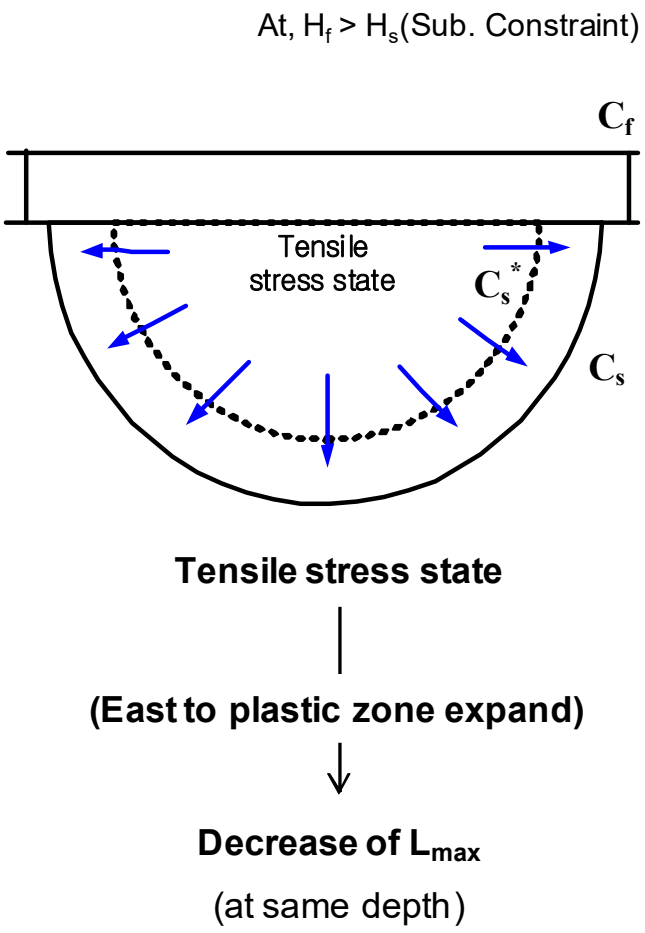

Figure 3.5. Load differences due to the interface at positive constraint

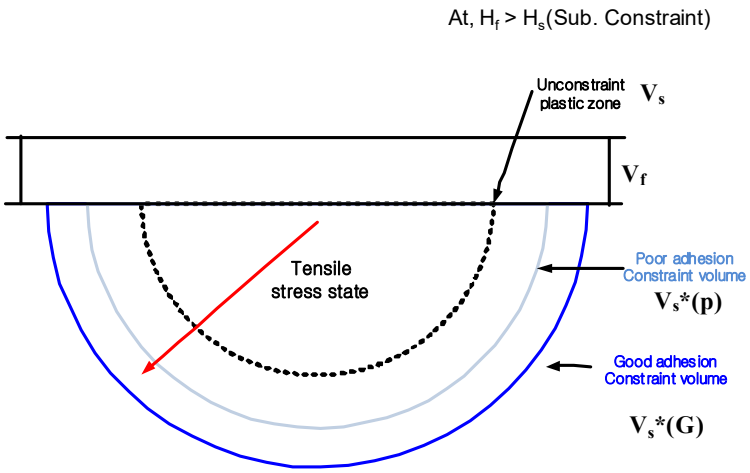

Figure 3.6. Change in volume difference according to adhesion at positive constraint

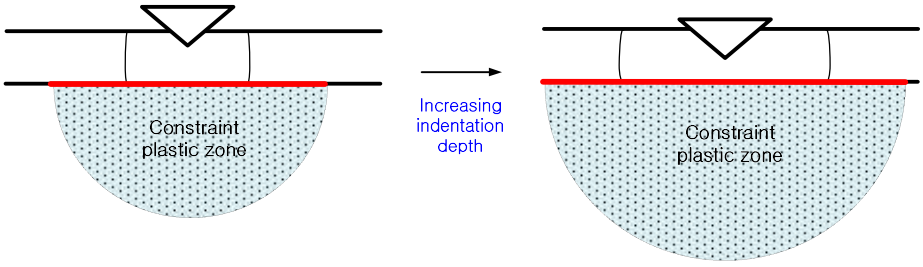

Fig. 3.7. Normalization volume

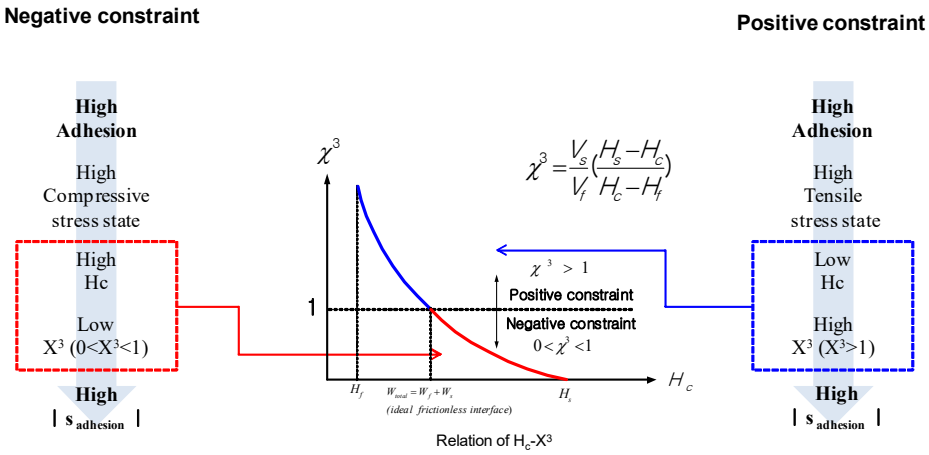

Figure 3.8. Relation of parameter at film constraint

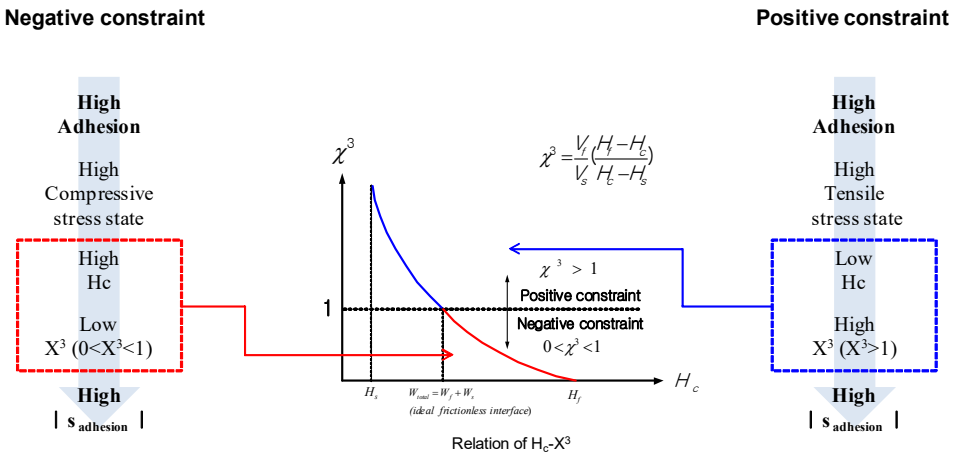

Figure 3.9. Relation of parameter at substrate constraint

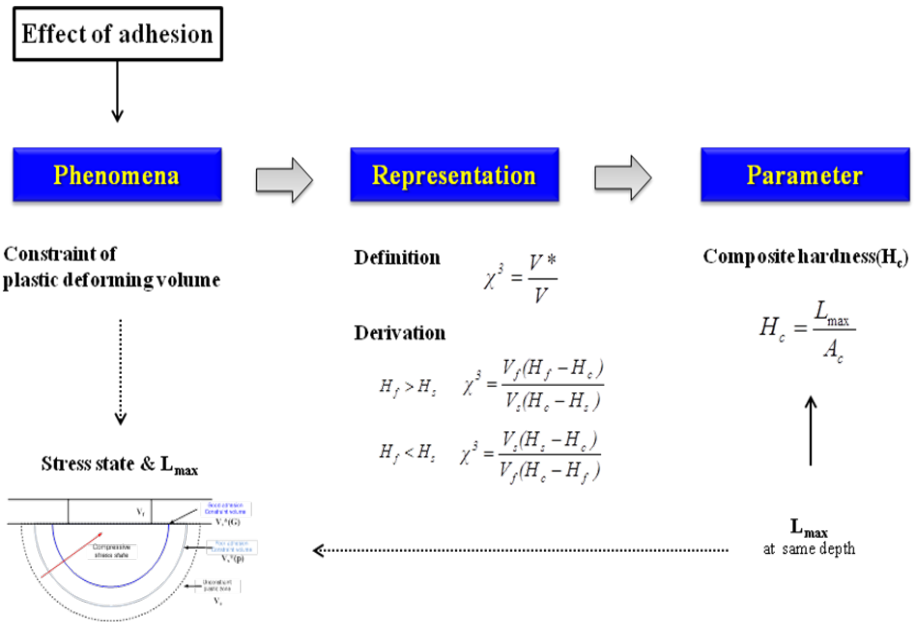

Figure 3.10. Relation of phenomena and indentation parameter

Chapter 4

VERIFICATION OF MODELS

Contents

4.1. Experimental Details

In order to verify the modeling determined above, tests were conducted on various thin film types. A thin film having a metal film and a polymer film was prepared, respectively, and adhesion strength evaluation was performed on the thin film. Also, in order to verify the adhesion determined through the indentation test, a scratch test and a pull-off test, respectively, were used.

4.1.1. Sample preparation

- Sample 1. Cu, Al substrate, MoW, NiO film

MoW, NiO film and Cu, Al substrate were used for verification of adhesion model. First of all, a Cu, Al was compaction for 2 days at 600 degrees in order to reduce the shrinkage at a high temperature. And the IPA(isopropyl alcohol) was 15 minutes into the ultrasonic cleaning. Substrate pretreatment conducted by controlling the surface treatment time in AR plasma atmosphere. Substrate pretreatment time is increased

to 5 minutes(10, 15, 20, 25, 30 min.). Other conditions were the same. (Ar 20sccm, 100W RF power, Working pressure:350mTorr, Temperature:350℃). After that film was deposited by a sputtering. During deposition, 30 sccm of Ar, D.C 600V, 300mTorr Working pressure during the deposition of the film was maintained. And deposited at 300 ℃ for 10 minutes was produced film thickness of 2 um. Finally, Ten samples were prepared having a different adhesion property.

- Sample 2. Glass, Cu, Al substrate, PVA, PDMS, PMMA film

PVA, PDMS, PMMA film and glass wafer, Cu, Al substrate were used for verification of adhesion model. First of all, a glass wafer, Cu, Al were compaction for 2 days at 600 degrees in order to reduce the shrinkage at a high temperature. And the IPA(isopropyl alcohol) was 15 minutes into the ultrasonic cleaning. The spin coating time was increased over 5 steps to give a change in adhesion strength at the interface. The thickness of the produced film is 6500, 4500, 4500nm, respectively, and 45 samples were obtained

4.1.2. Experiment conditions

For nanoindentation experiments we used a nanoindentation instrument, UNHT(CSM Instruments., Switzerland) and Nano Stress Mapper (Frontics Inc., Korea) with high load(depth) resolution. Fig. 4.1. shows the equipment. Indentation test was used in the form of a flat-end vickers indenter. Depth-control nanoindentation test was performed thin film having a thickness of 2 um in order to evaluate the "film-only hardness". Loading/unloading rate as 200 nm/min, holding time was set to 0S. Also, depth-control nanoindentation test was performed substrate having a thickness of 2 um in order to evaluate the "substrate-only hardness". To measure the composite hardness, RID(Relative Indentation Depth) was determined to be 0.4. RID is film thickness and indentation depth ratio. As shown in fig. 4.2, the effect of the film generated at RID<1. As the indentation depth increases to generate the effect of interface and substrate. Generally, Increasing the effect of the substrate in the RID>1 and delamination occurs in the film or interface. In the experimental conditions, between RID:1 and RID:0.1 is generated of the interface effect is important. Among them, composite hardness tests were performed on the RID 0.4. loading & unloading rate is 550nm / min,

holding time was fixed to 0S. Through three experiments, film/substrate/composite hardness and film/substrate plastic deforming volume were evaluated. Interface parameter obtained by using the test results. It evaluated the constrained plastic volume by the interface parameter. Finally, the adhesion strength was obtained with an interface parameter.

4.2. Results & Discussion

4.2.1. Comparison with scratch test and pull-off test

The scratch test method is specific types of a peel test. Apply a horizontal load while applying a constant vertical load to the scratch tip, and check the delamination point of the interface. From that point, we determine the critical load using the scratch length and load, and define it as the degree of adhesion. A schematic diagram of the scratch test is shown in Figure 4.3. The pull-off test determines the load at the time when the interface is separated by applying uniaxial stress to the specimen, as in the tensile test. The pull-off strength is evaluated using the determined load and the surface area of the specimen, and it is widely used for relatively soft films such as polymers. A schematic diagram of the pull-off test is shown in Figure 4.4.

4.2.2. Indentation parameter

I. Hardness ratio

The inherence hardness value of MoW film and Cu substrate obtained from indentation load-displacement curve in fig. 4.5. The hardness was calculated using the formula in chapter 3. The hardness of the MoW film was 4,405 MPa, glass substrate was evaluated by 486 MPa. Because of the substrate hardness is lower than the MoW film hardness, the plastic deforming volume of the substrate is constrained.

II. Elastic modulus/yield strength ratio

We have obtained the h_{max} and h_f values needed to obtain the E/Y ratio in the load-displacement curve of film and substrate. E/Y ratio and indentation depth parameter in previous studies have the following formula relationship. $E/Y = 44.81*h_{max}/(h_{max}-h_f)-27.78$. MoW in the plastic zone radius is 2,919nm, glass substrate of the plastic zone radius is 4,216nm in RID 0.4.

Considering the above two situations, relatively film is hard and small plastic zone than substrate. so, we can be predicted substrate constrained by MoW film in the negative direction. Fig. 4.6 shows a schematic diagram constrained situation.

4.2.3. Indentation adhesion strength

Derive each key factor and compared to tendency of the theoretical analysis as described in chapter 3. Key parameter is L_{max}, composite hardness, interface parameter, work of adhesion, adhesion strength. To get a indentation load-displacement curve through the test with species with different adhesion sample.

The indentation depth of each of the curves is constant, however, maximum load can be seen a tendency to increase as the adhesion force is increased.(as the increase in 0 minute to 30 minutes. The reason for increasing the maximum load is increase the plastic constrained volume in the negative direction. It causes increase of compressive stress inside a film. so, maximum load is increased at same indentation depth.

Hardness have a tendency such as the maximum load independently of the influence of the contact area. Because of the contact

area is not a major factor, the maximum load and composite hardness trend is same.

Interface parameters calculated using eq. (3-18). The better adhesion sample can be identified by having a value that converges to 0. Interface parameter as a factor representing the relative degree to which constraint plastic volume of soft material. The interface parameter that converge to zero means that the constraint volume is increased. The better adhesion can be confirmed that the amount of increase in volume constraining.

The work of adhesion is obtained by using eq. (3-26). The better adhesion specimens can be confirmed that the work of adhesion increases. However, this value is depend on the indentation depth. Thus not a quantitative adhesion values.

Evaluation of adhesion strength using eq. (3-31) and the pre-processing time to increase the substrate confirmed increasing adhesion property. For the case of film negative constraint sample, having better adhesion property, increases of maximum load and composite hardness. Film plastic constrained volume assessed using the interface parameter. Work of adhesion was evaluated through the interface parameter. Normalization by previous constraint volume of film. Quantitative

adhesion strength was obtained independent of the experimental conditions.

4.2.4. Experimental results

1) Metallic film

In Fig. 4.7, and 4.8., the results of the indentation test and the scratch test can be confirmed for the metal film. It can be seen that as the adhesion at the interface increases, the critical load of scratch test and the adhesion strength of the indentation test increases, and in particular, as pretreatment time of the substrate surface increases, the difference increases. In figure 4.9. and 4.10., it is possible to check the adhesion strength to other film materials on the same substrate. It can be seen that the overall adhesion value on the harder substrate is large.

2) Polymer film

In Fig. 4.11,, 4.12. and 4.13., the results of the indentation test and the scratch test can be confirmed for the metal film. It can be seen that as the adhesion at the interface increases, the critical load of scratch test and the adhesion strength of the indentation test increases, and in particular, as pretreatment time of the substrate surface increases, the difference increases. In figure 4.14., 4.15. and 4.16., it is possible to check the adhesion strength to other film materials on the same substrate. It can be seen that the overall adhesion value on the harder substrate is large.

Figure 4.17. shows the adhesion strength to the entire polymer film. In general, it can be seen that the PMMA film having a higher hardness value has a higher adhesion strength, and it can be seen that the difference according to the rate becomes more pronounced as it has a higher hardness.

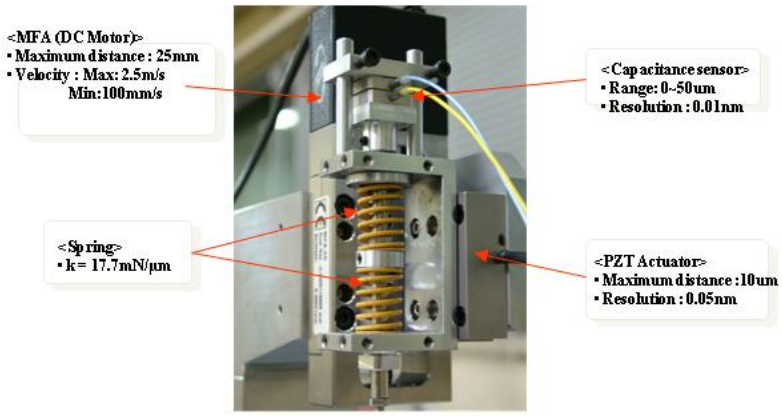

(a)

(b)

Figure 4.1. Commercial nano-indenter: (a) Nano Stress Mapper and (b)

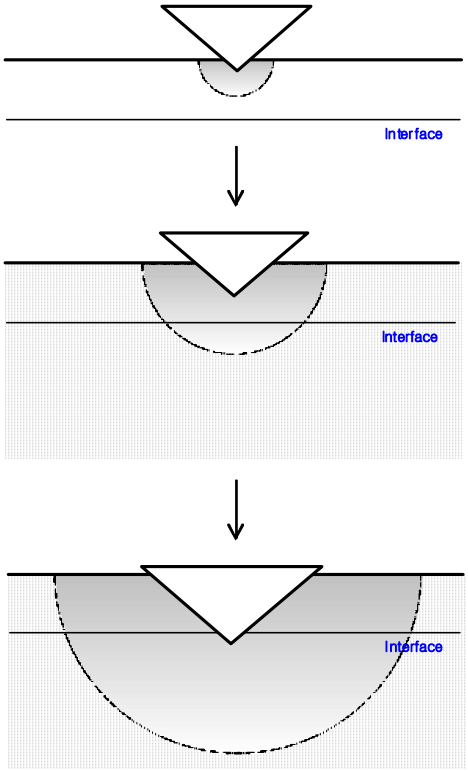

Step 1. **RID < 0.1**
- $W_{total} = W_{film}$
- Dominant factor : Film

Step 2. **0.1< RID < 1**
- $W_{total} = W_{film} + W_{adhesion} + W_{substrate}$

Step 3. **RID > 1**
- $W_{total} = W_{film} + W_{adhesion} + W_{substrate}$
- Dominant factor : Substrate

- Possibility of interfacial delamination

figure 4.2. Indentation depth dependency

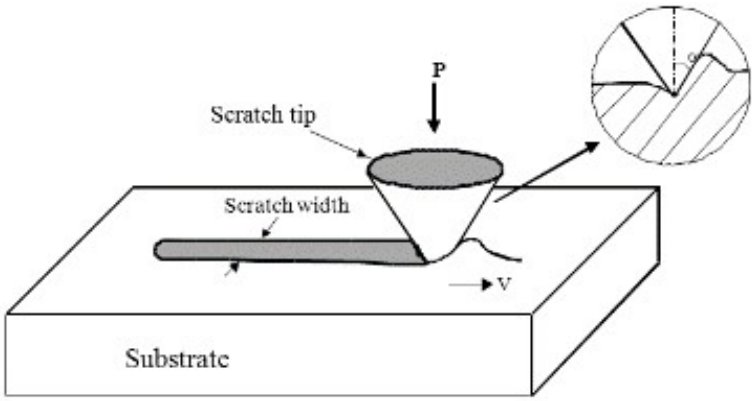

(a)

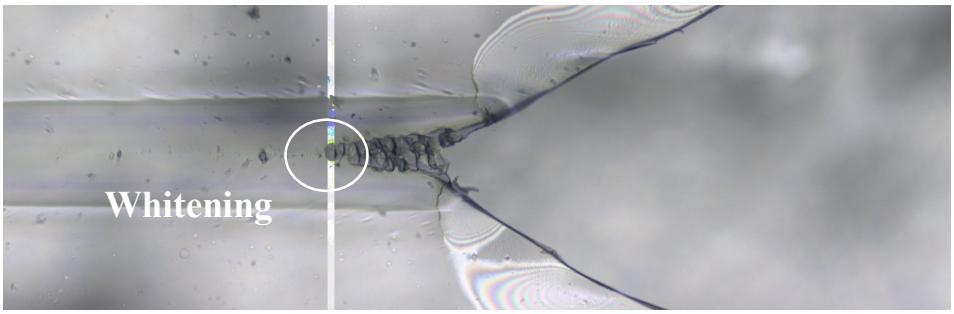

(b)

Figure 4.3. Scratch test method: (a) Schematic diagram and (b) Real-time image

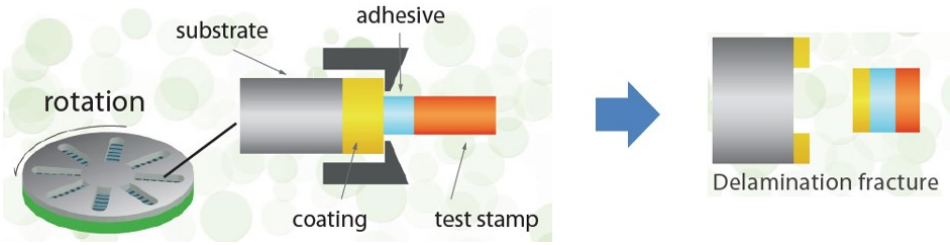

Figure 4.4. Schematic diagram of pull-off test

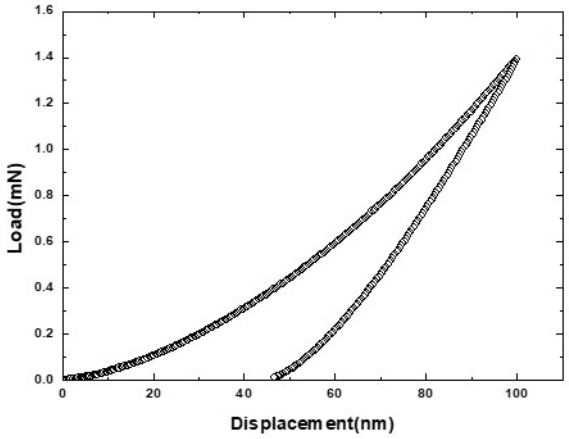

(a)

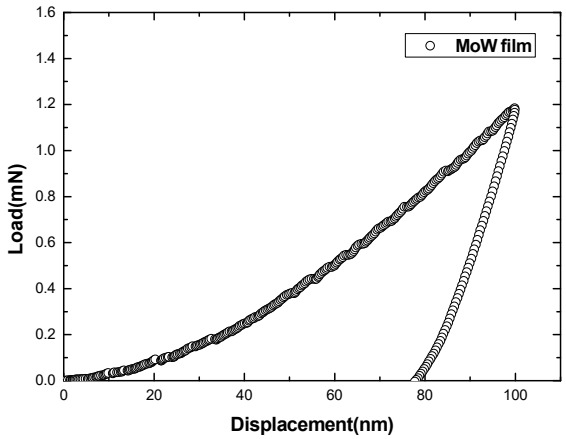

(b)

Figure 4.5. Indentation load-displacement curve:

(a) Cu substrate and (b) MoW film

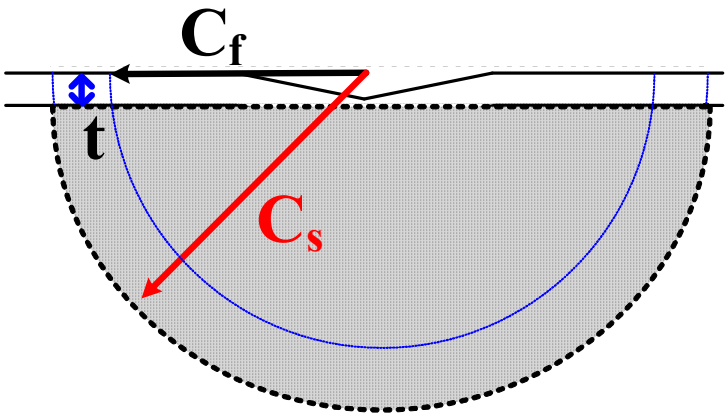

Figure 4.6. Constraint condition of MoW film at the beneath indenter

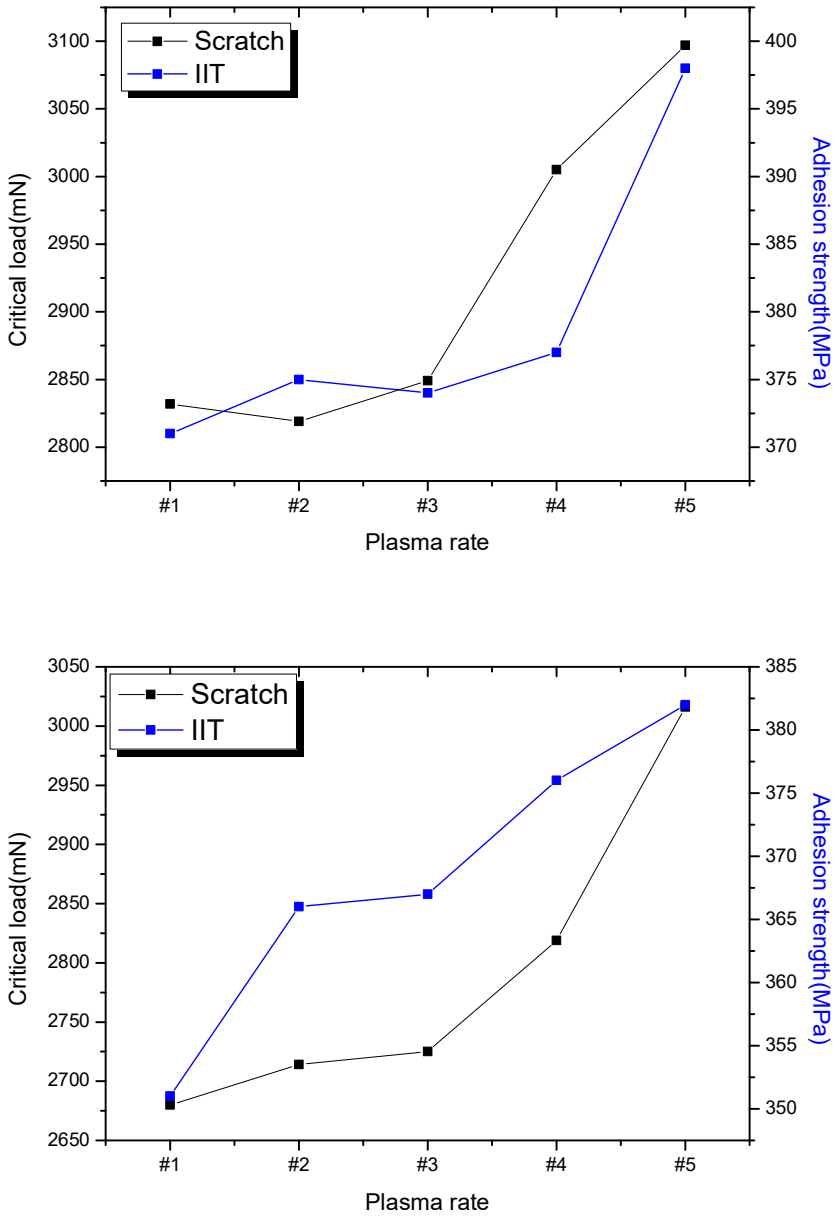

Figure 4.7. Comparing indentation and scratch test results(MoW film)

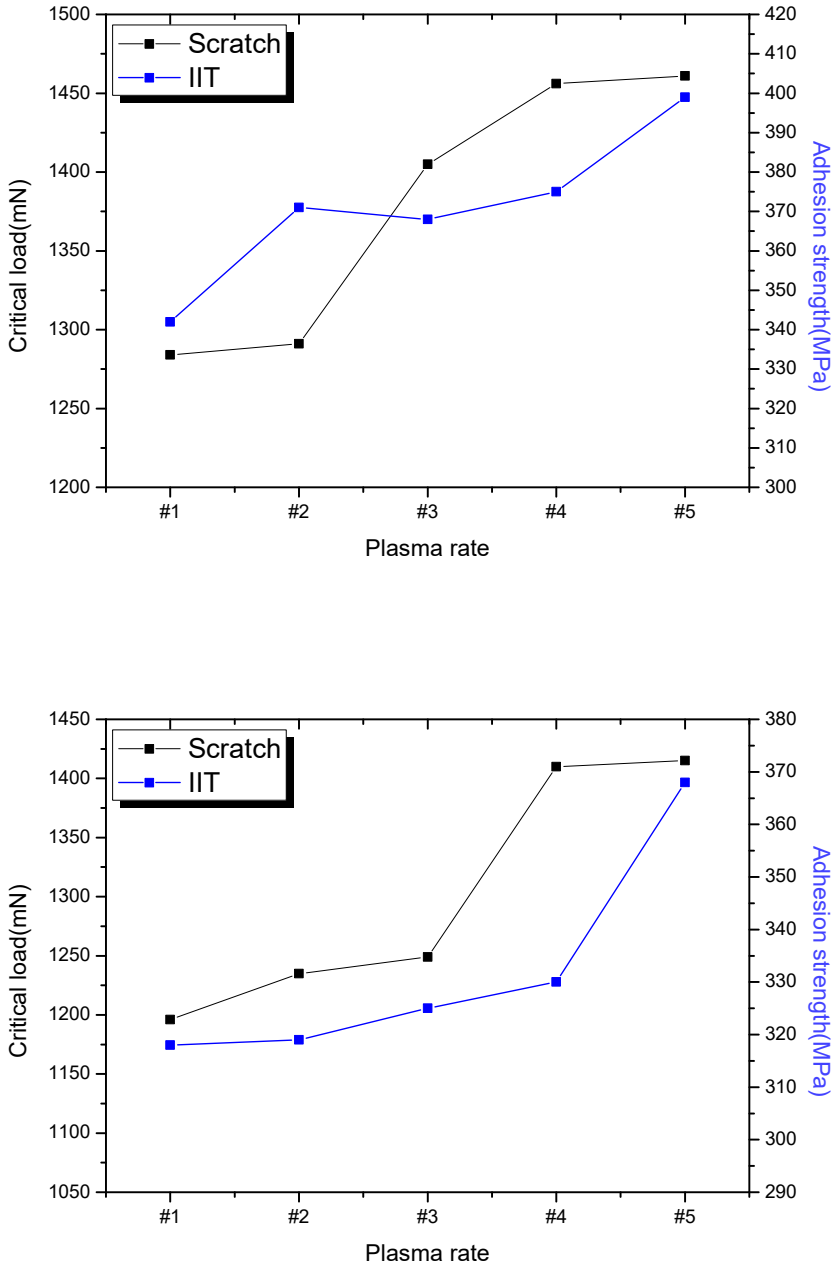

Figure 4.8. Comparing indentation and scratch test results(NiO film)

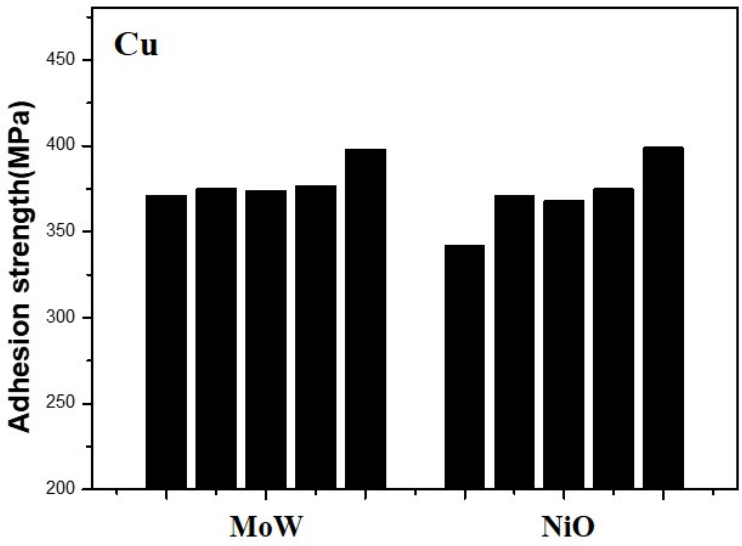

Figure 4.9. Adhesion according to film materials(Cu substrate)

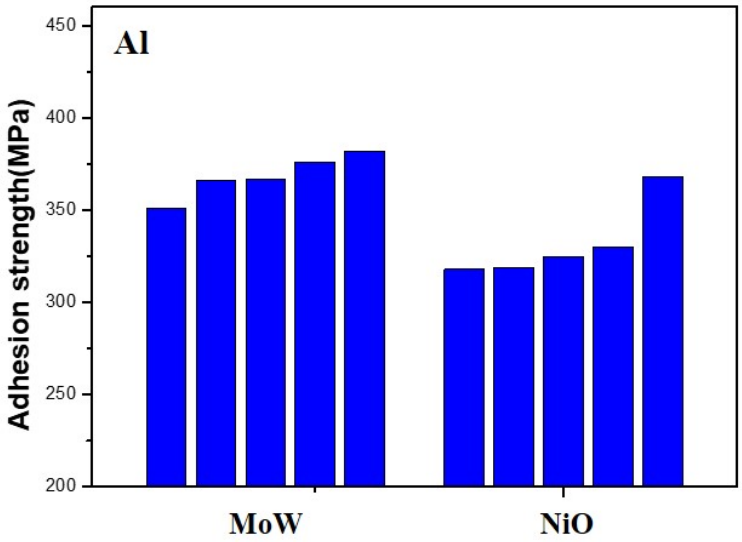

Figure 4.10. Adhesion according to film materials(Al substrate)

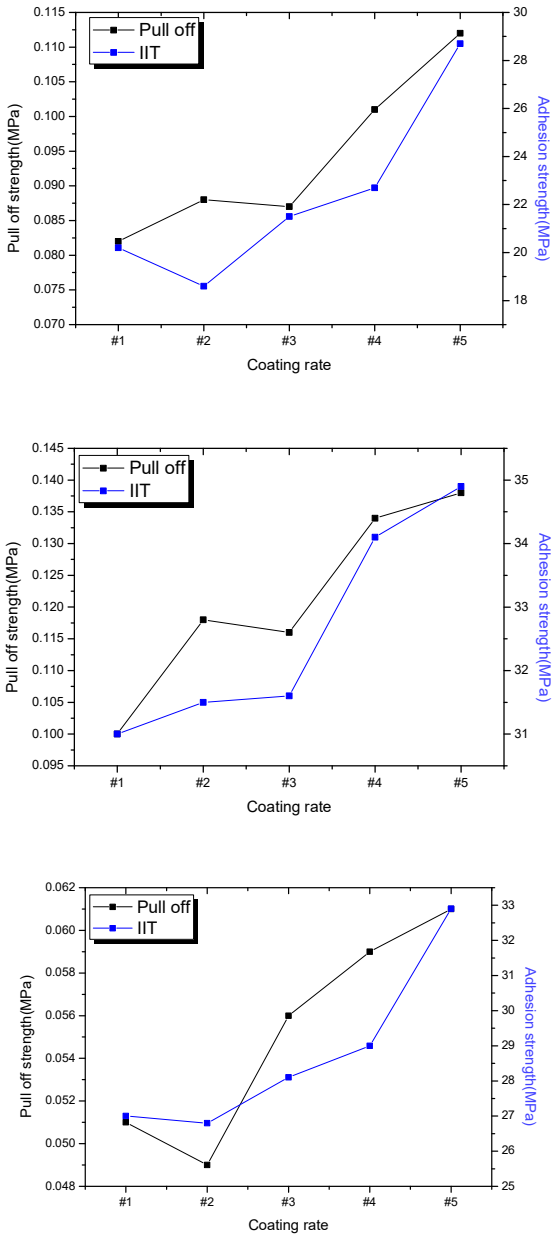

Figure 4.11. Comparing indentation and pull-off test results(PVAfilm)

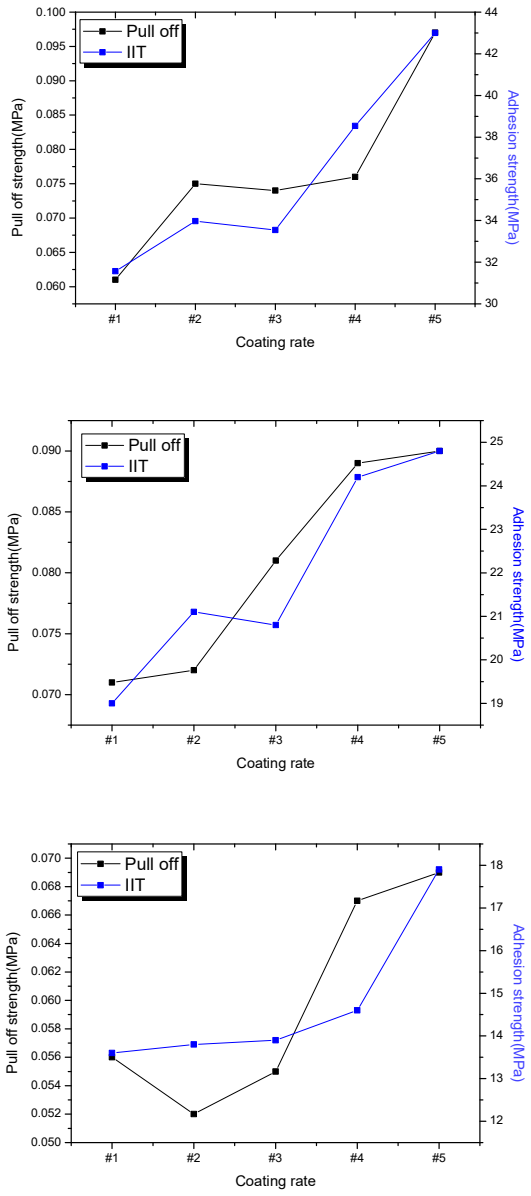

Figure 4.12. Comparing indentation and pull-off test results(PDMSfilm)

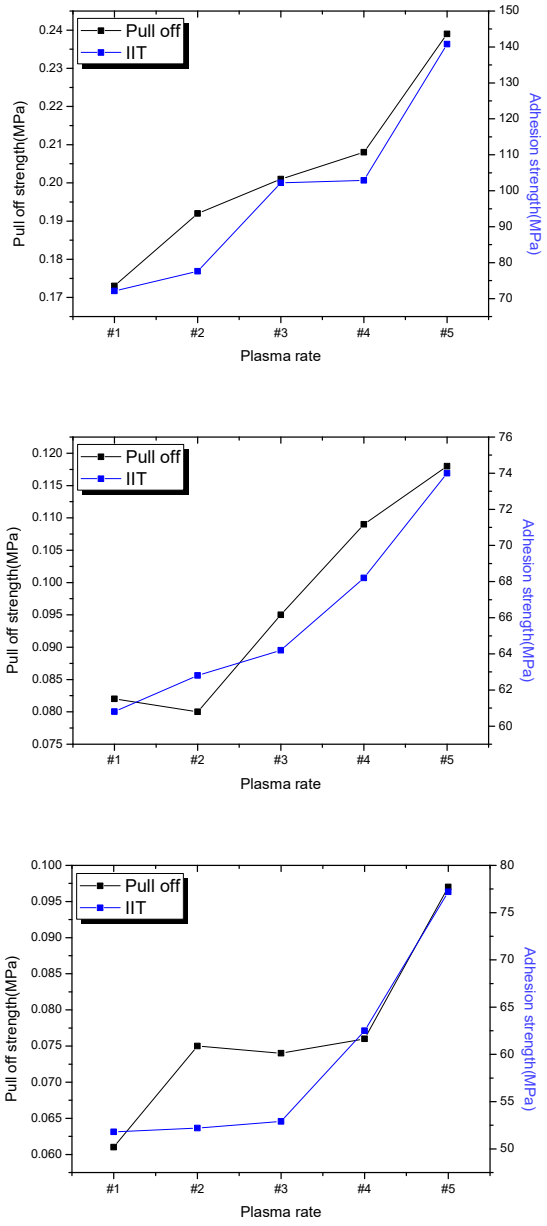

Figure 4.13. Comparing indentation and pull-off test results(PMMAfilm)

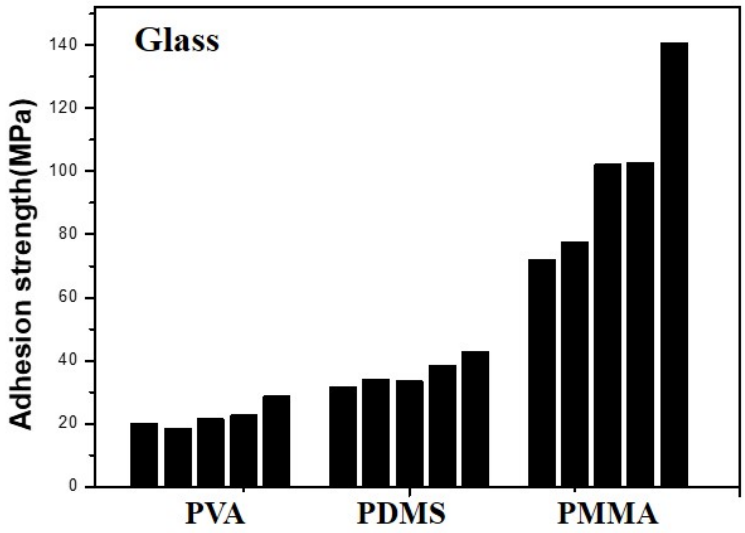

Figure 4.14. Adhesion according to film materials(Glass substrate)

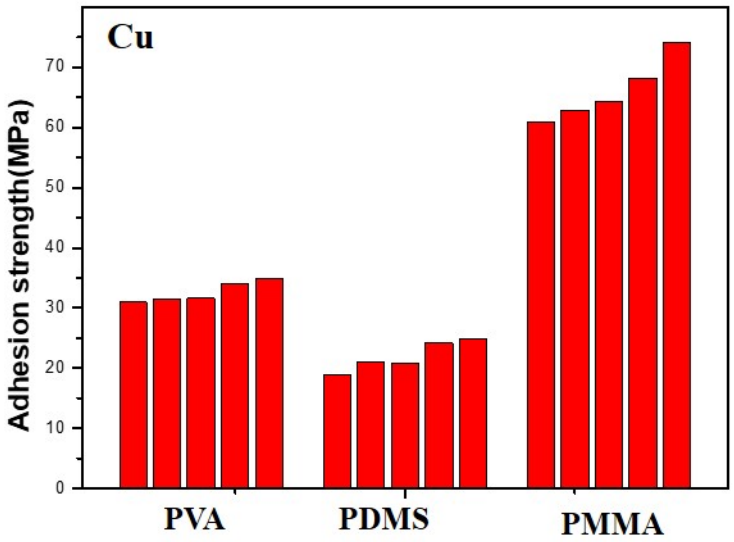

Figure 4.15. Adhesion according to film materials(Cu substrate)

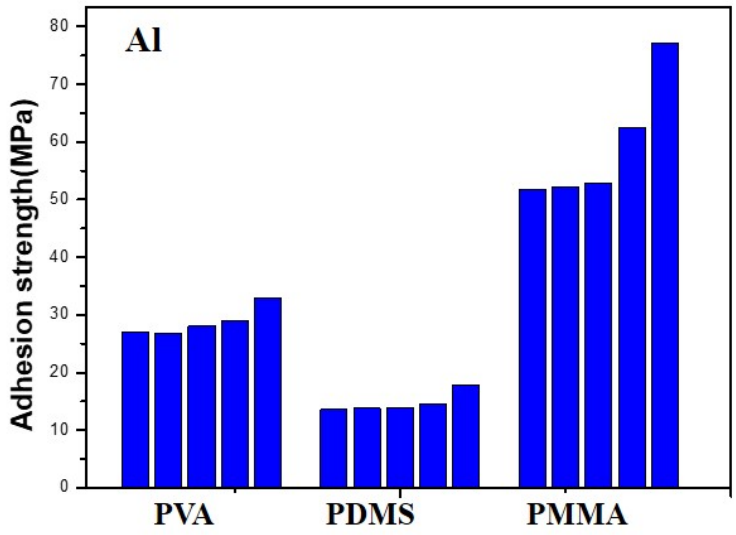

Figure 4.16. Adhesion according to film materials(Al substrate)

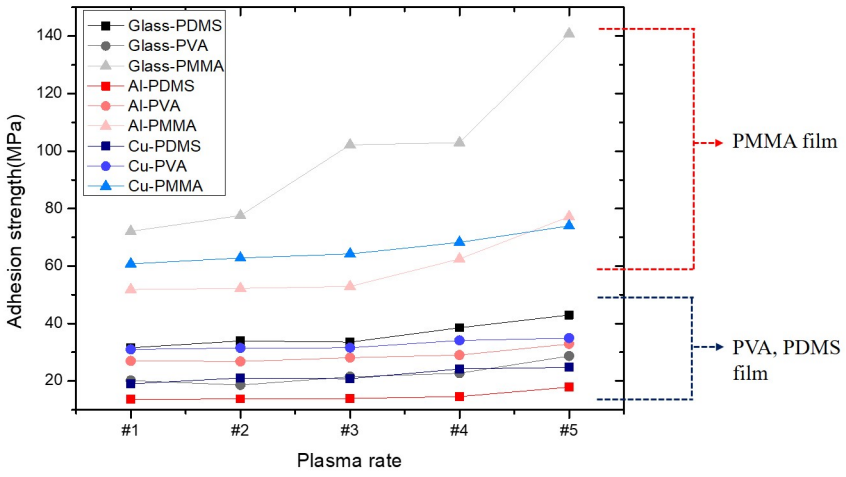

Figure 4.17. Change of adhesion strength according to interface condition

Chapter 5

CONCLUSION

Evaluation of single layer thin-film adhesion strength is proposed using the indentation test. The proposed method solves the three limitations with the conventional test methods. First, it was quantitatively considering the effect of the thin film and the substrate. Second, expanded the applicability of the material. Third, proposed a method that does not need the optical observation.

At the indentation test, hemispherical plastic zone is generated beneath the indenter and extended indentation depth increases. In the thin-film system, plastic zone that extends as the indentation depth increases, constrained relatively soft material by the interface effect. The constraint volume different depending on the adhesion strength. Define the interfacial constraint effect by the influence of the interface, which was derived by mathematically. The amount of constraint volume is increase as good adhesion properties. Additionally, modeling for work of film and substrate plastic deformation effect at indentation test condition using the formulated hardness. Indentation load-displacement curve that contained the film/substrate/interface effect analysis though the *'interfacial constraint effect'* and *'formulated hardness'*.

The following are the central results of the work.

1. Increasing the indentation depth, the expanding plastic zone is constraint by interface. Relatively soft materials are constrained by relatively hard materials. So, the constraint materials are determined from the hardness ratio of the thin films and substrates. And plastic zone radius determined by E/H ratio has 2 different case to find in thin film/substrate system. In other words, constrained materials are determined by hardness ratio and the constrained directions are determined by the elastic modulus/hardness ratio. There are 4 situations beneath of the indenters considering constrained materials and directions.

2. The relatively better adhesion makes increased constraint volume with decreased interfacial slips. Interface parameter (χ^3) is proposed to express constraint volume of relatively soft materials. 'χ^3' shows plastic volume changes by interface. Definition of interface parameter is ratio of the volume before constraint to the volume after constraint. Through this interface parameter, the

constraint volume change is modeled. The interface parameter derived using the *Expanding Cavity Model* and *formulated hardness*.

3. The expanding plastic volume is constrained by the interface.

   - Positive constraint : Positive constraint gets limitation on the deformation of reduction by adhesion. It causes tensile stress in the relatively soft material. As it gets better adhesion, greater plastic volume is constrained, resulting higher tensile stress state. Then the measured load gets lower at the same indentation depth as it has better adhesion.

   - Negative constraint : Negative constraint gets limitation on the deformation of expansion by adhesion. It causes compressive stress in the relatively soft material. As it gets advanced adhesion, greater plastic volume is constrained, resulting higher compressive stress state. Then the measured load gets higher at the same indentation depth as it has better adhesion.

This analysis results in main factor is the difference in the indentation load at same depth.

4. Calculated work of adhesion through modelling increases as the indentation depth increases. Because the area effect by interface becomes larger as the indentation depth increases. To derive quantitative work of adhesion regardless of the condition of test, normalization is needed. It is the work done to constrain plastic volume. Therefore, quantitative value is derived from normalizing plastic volume before constraint. Finally, adhesion strength is derived from normalizing with the volume before constraint.

5. Models were comparing scratch and pull-off test for verification. It was deposited on a hard substrate with soft film. The adhesion strength was varied through a substrate pre-treatment. It was confirmed that the results of both tests have the similar tendency. In addition, a variety of materials were evaluated for adhesion by

indentation test.

References

[1] D. S. Campbell, in L. I. Maissel and R. Glang (eds.), Handbook of Thin film Technology, McGraw-Hill, New York, 1970, Chap. 12.3.S. Suresh, A.E. Giannakopoulos, *Acta Mater.* 46, 5755 (1998).

[2] S.V. Hainsworth, *Surface and Coatings Technology.,* 163-164 (2003).

[3] Chaiwut Gamonpilas , *MSEA.,* 380 (2004).

[4] H. Li, *Scripta Materialia.,* 45 (2001).

[5] Jeong-Hoon Ahn, *MSE*., 285 (2000).

[6] D.M. Lipkin, D.R. Clarke, and A.G. Evans, *Acta Mater*., 46 (1998).

[7] A. Furuya, N. Hosoi, and Y. Ohshita, *J. Appl. Phys*., 78 (1995).

[8] C. Lee and K. Lin, *Japan J. Appl. Phys*., 33 (1994).

[9] A. Bagchi, G. Lucas, Z. Suo, and A.G. Evans, *J. Mater. Res*., 9 (1994).

[10] A.G. Evans and J.W. Hutchinson, *Int. J. Solids struc.,* 20, 5 (1984).

[11] D.B. Marshall and A.G. Evans, *J.Appl. Phys*., 56 (1984).

[12] P. Benjamin and C. Weaver, *Proc. R. Soc. London*, A254 (1960).

[13] P. Burnett and D. Rickersby, *Thin Solid Films*, 154 (1987).

[14] S. Venkataraman, D. Kohlstedt, and W.W. Gerberich, *J. Mater. Res*.,

8 (1993).

[15] D.S. Venkataraman, D. Kohlstedt, and W.W. Gerberich, *J. Mater. Res*., 7 (1992).

[16] V. Tvergaard and J.W. Hutchinson, *J. Mech. Phys. Solids*, 44 (1996).

[17] Z. Suo and J.W. Hutchinson, *Mater. Sci. Eng*., A107 (1989).

[18] M. Menningen and H. Weiss, *Surf. Coat. Tech*., 76-77 (1995).

[19] *ASTM standard* 399-90 (1990).

[20] J. Vlassak and W. Nix, *J. Mater. Res.,* 7 (1992).

[21] H. Hertz. *J.Reine Angew. Math*. 92, 156 (1881).

[22] H. Hertz. *Verh. Ver. Beförderung Gewerbe Fleisses* 61, 410 (1882).

[23] A.C. Fisher-Cripps. *J. Mater. Res*. 16, 3050 (2001).

[24] I.N. Sneddon. *Proc. Camb. Philos. Soc*. 44, 492 (1948).

[25] J.R. Barber, D.A. Billings. *Int. J. Mech. Sci.* 32, 991 (1990).

[26] G.G. Bilodeau. *J. App. Mech.* 59, 519 (1992).

[27] F. Auerbach. Ann. *Phys. Chem*. 43, 61 (1891).

[28] E. Meyer. *Phys. Z* 9, 66 (1908).

[29] S.L. Hoyt. *Trans. Am. Soc. Steel Treat*. 6, 396 (1924).

[30] M.C. Shaw. *The Science of Hardness Testing and its Research Applications* (J.H. Westbrook and H. Conrad Eds., American Society for Metals, Cleveland, 1973).

[31] M.V. Swain, J.T. Hagan. *J. Phys. D: Appl. Phys*. 9, 2201 (1976).

[32] M.T. Huber. *Ann. D. Physik* 14, 153 (1904).

[33] K.L. Johnson. *Contact Mechanics* (Cambridge University Press, Cambridge, 1985).

[34] R. Hill, E.H. Lee, S.J. Tupper. *Proc. R. Soc. Lond. A* 188, 273 (1947).

[35] R. Hill. *The Mathematical Theory of Plasticity* (Clarendon Press, Oxford, 1950).

[36] D.M. Marsh. *Proc. R. Soc. Lond. A* 279, 420 (1964).

[37] L.E. Samuels, T.O. Mulhearn. *J. Mech. Phys. Sol*. 5, 125 (1957).

[38] T.O. Mulhearn. *J. Mech. Phys. Sol*. 7, 85 (1959).

[39] K.L. Johnson. *J. Mech. Phys. Sol*. 18, 115 (1970).

[40] M.C. Shaw, D.J. DeSalvo. *J. Eng. Ind. Trans. ASME* 92, 469 (1970).

[41] M.C. Shaw, D.J. DeSalvo. *J. Eng. Ind. Trans. ASME* 92, 480 (1970).

[42] C. Hardy, C.N. Baronet, G.V. Tordion. *Int. J. Numer. Methods Eng*. 3, 451 (1971).

[43] C.M. Perrott. *Wear* 45, 293 (1977).

[44] S.S. Chiang, D.B. Marshall, A.G. Evans. *J. Appl. Phys.* 53, 281 (1982).

[45] S.S. Chiang, D.B. Marshall, A.G. Evans. *J. Appl. Phys*. 53, 312 (1982).

[46] J.B. Pethica. *Third International Conference on Modification of Surface Properties of Metals by Ion-Implantation* (V. Ashworth et al. Eds., Pergammon Press, Oxford, 1982).

[47] J.S. Field. *Surf. Coat. Technol*. 36, 817 (1988).

[48] N.A. Stillwell, D. Tabor. *Phys. Proc. Soc*. 78, 169 (1961).

[49] B.R. Lawn, V.R. Howes. *J. Mater. Sci*. 16, 2745 (1981).

[50] S.I. Bulychev, V.P. Alekhin, M.Kh. Shorshorov, A.P. Ternorskii. *Zavod*. Lab. 41, 11137 (1975).

[51] J.L. Loubet, J.M. Georges, O. Marchesini, G. Meille. *J. Tribol*. 106, 43 (1984).

[52] T.J. Bell, A. Bendeli, J.S. Field, M.V. Swain, E.G. *Thwaite. Metrologia* 28, 463 (1991).

[53] J.S. Field, M.V. Swain. *J. Mater. Res.* 8, 297 (1993).

[54] A.C. Fisher-Cripps. *J. Mater. Res.* 16, 1579 (2001).

[55] H.M. Pollock. *ASM Handbook, Friction, Lubrication, and Wear Technology* 18, 419 (1992).

[56] J.L. Hay, G.M. Pharr. *ASM Handbook, Materials Testing and Evaluation* 8, 232 (2000).

[57] S.A. Syed, K.J. Wahl, R.J. Colton. *Mater. Res. Soc. Symp. Proc.* 594, 471 (2000).

[58] G.M. Pharr, A. Bolshakov. *J. Mater. Res*. 17, 2660 (2002).

[59] I.N. Sneddon. *Int. J. Engng. Sci.* 3, 47 (1965).

[60] A.E.H. Love. *Quart. J. Math*. 10, 161 (1939).

[61] A.E.H. Love. *Phil. Trans. A* 228, 377 (1929).

[62] J.W. Harding, I.N. Sneddon. *Proc. Camb. Phil. Soc.* 41, 16 (1945).

[63] I.N. Sneddon. *Fourier Transforms* (McGraw-Hill, New York, 1951).

[64] G.M. Pharr, W.C. Oliver, F.R. Brotzen. *J. Mater. Res*. 7, 613 (1992).

[65] C.M. Cheng, Y.T. Cheng. *Appl. Phys. Lett*. 71, 2623 (1997).

[66] H. Gao, T.W. Wu. *J. Mater. Res*. 8, 3229 (1993).

[67] T.Y. Tsui, W.C. Oliver, G.M. Pharr. *J. Mater. Res*. 11, 752 (1996).

[68] Y.H. Lee, D. Kwon. *J. Mater. Res*. 17, 901 (2002).

[69] Y.H. Lee, D. Kwon. *Acta Mater.* 52, 1555 (2004).

[70] G.M. Pharr, D.S. Harding, W.C. Oliver. *Mechanical Properties and Deformation Behavior of Materials Having Ultra-Fine Microstructures* (Kluwer Academic Publishers, Netherlands, 1993).

[71] B.R. Lawn, A.G. Evans, D.B. Marshall. *J. Am. Ceram. Soc*. 63, 574 (1980).

[72] B.R. Lawn, R. Wilshaw. *J. Mater. Sci*. 10, 1049 (1975).

[73] A.G. Evans, E.A. Charles. *J. Am. Ceram*. Soc. 59, 371 (1976).

[74] B.R. Lawn, D.B. Marshall. *J. Am. Ceram*. Soc. 62, 347 (1979).

[75] P. Chantikul, G.R. Anstis, B.R. Lawn, D.B. Marshall. *J. Am. Ceram. Soc*. 64, 539 (1981).

[76] X. Li, D. Diao, B. Bhushan. *Acta Mater*. 45, 4453 (1997).

[77] J.S. Lee, J.I. Jang, B.W. Lee, Y. Choi, S.G. Lee, D. Kwon. *Acta Mater*. 54, 1101 (2006).

[78] G.R. Antis, P. Chantikul, B.R. Lawn, D.B. Marshall. *J. Am. Ceram. Soc*. 64, 533 (1981).

[79] J.A. Knapp, D.M. Folstaedt, S.M. Myers, J.C. Barbour, T.A. Friedmann. *J. Appl. Phys*. 85, 1460 (1999).

[80] J.A. Knapp, D.M. Folstaedt, S.M. Myers, J.C. Barbour, T.A. Friedmann, J.W. Ager Ⅲ, O.R. Monteiro, I.G. Brown. *Surf. Coat. Technol*. 103-104, 268 (1998).

[81] S. Jayaraman, G.T. Hahn, W.C. Oliver, C.A. Rubin, P.C. Bastias. *Int. J. Solids Struct*. 35, 365 (1998).

[82] D. Tabor. *The Hardness of Metals* (Clarendon Press, Oxford, 1951).

[83] M.F. Doerner, W.D. Nix. *J. Mater. Res*. 1, 601 (1986).

[84] W.C. Oliver, G.M. Pharr. *J. Mater. Res*. 7, 1564 (1992).

[85] A. Bolshakov, G.M. Pharr. *J. Mater. Res*. 13, 1049 (1998).

[86] M. Dao, N. Chollacoop, K.J. Van Vliet, T.A. Venkatesh, S. Suresh.

Acta Mater. 49, 3899 (2001).

[87] A.K. Bhattacharya and W.D. Nix, *Int. J. Solids Struct*. 24, 1287 (1988).

[88] B.D. Fabes, W.C. Oliver, R.A. McKee, and F.J. Walker, *J. Mater. Res.* 7, 3056 (1992).

[89] H.F. Wang, X. Yang, H. Bangert, P. Torzicky, and L. Wen, *Thin Solid Films* 214, 68 (1992).

[90] D. Tabor, 1986. *Indentation hardness and its measurement: some cautionary comments*. In: Blau, P.J., Lawn, B.R. (Eds.), *Mircoindentation Techniques in Materials Science and Engineering, ASTM STP 889, ASTM Press*, Philadelphia, pp. 129-159.

[91] B.R. Lawn, *J. Amer. Ceram. Soc*. 81, 115 (1998).

[92] A.E. Giannakopoulos, S. Surech, *Scripta Mater.* 40, 1191 (1999).

[93] W. Zhang, G. Subhash, *Int. J. Solids Struct.* 38, 5893 (2001).

[94] M. Mata, M. Anglada, J. Alcala, *Philos. Mag. A* 82, 1831 (2002).

[95] M. Mata, J. Alcala, *J. Mater. Res*. 18, 1705 (2003).

[96] A.C. Fisher-cripps, *J. Mater. Res.* 32, 727 (1997).

[97] S.D. Mesarovic, N.A. Fleck, *Proc. R. Soc. Lond. A* 455, 2707 (1999).

[98] Y.J. Park, G.M. Pharr, *Thin Solid Films* 447, 246 (2004).

[99] X.-L. Gao, X.N. Jing, G. Subhash, *Int. J. Solids Struct.* 43, 2193

(2006).

초 록

산업화가 다양해지고 고도화가 될수록 국가기간 산업에서는 다양한 역할 및 특성을 가지고 있는 소재를 요구하고 있다. 특히 전자, 디스플레이 등 첨단 산업에서는 이종소재를 접합시킨 다기능성 소재의 활용이 증가하고 있다. 하지만 이러한 이종소재의 접합은 물리, 화학적인 인위적 접합으로서 발생되는 계면은 박막과 모재에 비해 기계적인 특성이 상대적으로 취약한 부분으로 나타나며, 외부에서 응력이 가해지는 상황 또는 환경적 요인에 의해 박리와 파손이 우선적으로 발생한다. 그렇기 때문에 이러한 계면의 특성은 박막시스템의 신뢰성을 평가하는 최우선 요소로서 정량적으로 평가하기 위한 연구와 다양한 시험법들이 개발되었다. 그러나 기존의 시험법은 정량적으로 접착력을 평가하기에 몇가지 한

계점을 가지고 있다. 첫 번째로, 박막과 모재의 영향이다. 기존에 사용되어왔던 접착력 평가 시험법의 경우 시험법상 특수성으로 인해 필수불가결하게 박막과 모재의 특성이 결과값에 주도적으로 작용하게 된다. 하지만 아직까지 박막과 모재의 영향을 정량적으로 해석하는 연구가 미비하여 정확한 접착력을 평가하는데 문제점을 가지고 있다. 두 번째로는, 기존의 시험법이 해당 소재의 파괴를 가져온다는 점이다. 파괴 시험법으로서 가지는 한계점으로 수 나노미터 수준으로 경박화 되고 있는 박막시스템에서 정확한 계면 박리 시점 및 광학 장비를 통한 파손 영역의 관찰이 필수적이라는 점이다. 결국 정확한 박리 시점의 선택의 어려움과 매우 좁은 영역의 정확한 관찰이 동반되어야 목적으로 하는 접착력의 정확한 평가가 가능하다는 문제점을 가지고 있다. 세 번째로, 시험법에 따라 적용할 수 있는 소재가 제한되어 있어 적용상의 한계가 있다. 산

업에서 필요로 하는 소재는 시간이 지날수록 다양해지고 있다. 하지만 기존의 시험법이 적용 가능한 소재에 한계를 가지고 있으며, 결국 하나의 시험법을 통하여 다양한 소재에 대한 접착력 평가 및 결과 비교에 문제점을 가지고 있다고 할 수 있다.

본 학위 논문에서는 기존의 시험법들이 가지는 한계점을 극복하고자 비파괴 시험이 가능하고 박막과 기판의 영향을 정량화 시키기 위해 압입시험을 이용하여 접착력을 평가하는 모델을 연구하였다. 압입시험은 간단한 시험을 통해 압입자 하부의 응력 분포 및 상태를 해석함으로써 다양한 역학특성을 평가하는 최신의 기계적 시험법이다. 또한 높은 하중 분해능과 변위 분해능을 가지는 장비 개발을 통해 매크로, 마이크로 스케일 뿐만 아니라 나노 스케일 박막까지의 기계적 물성을 평가하는데 활용성이 증가하고 있다.

박막시스템에 압입시험을 수행하면 박막과 모재의 개별적인 하중변위 곡선을 얻을 수 있으며 이와 함께 계면의 영향이 복합적으로 반영이 된 압입 하중변위 곡선을 획득할 수 있다. 하지만 단순히 이렇게 얻은 곡선에서 박막과 모재의 영향을 실험적으로 구분하여 분리해 낼 수 없었기 때문에 이론적 모델링을 통해서 각각의 영향을 구분하였다.

본 연구에서는 압입시험 시 발생되는 에너지의 총합을 박막/계면/모재의 합으로 정의하고, 가해진 하중과 면적의 비로 정의되는 경도를 압입시험 시 발생된 에너지와 압입자 하부의 소성변형에 동반되는 부피의 비로 확장시킨 개념을 인용하였다. 확장된 경도를 바탕으로 박막과 모재의 변형에 의해 발생된 일을 각각 해석하였다. 또한 계면에 의해서 압입자 하부에 확장되는 소성역이 구속되는 상황을 해석하였다. 박막과 모재 중 상대적으로 연질의

재료가 경질의 재료에 의해 소성역이 구속됨을 가정하였고, 수치화를 위해 공극확장모델을 사용하여 수식을 전개하였다. 이를 통해 계면에 의해 상대적으로 연질 재료의 구속되는 부피의 양을 표현하는 계면인자를 정의하였고, 계면인자를 재료 인자를 이용하여 수학적으로 도출하였다. 압입시험에서 계면에 의한 구속효과를 해석하여 계면의 일의 양을 정량적으로 평가하는 수식을 제안하였으며, 압입깊이에 따라 달라지는 일의 양을 구속되는 부피로 정규화 하여 최종적으로 접착강도를 평가하는 수식을 제안하였다.

제안한 접착력 평가 모델의 타당성을 검증하기 위해 기존의 박리시험을 통해 얻어진 결과와 압입시험을 이용하여 도출된 접착강도를 비교하여 유사한 경향성을 확인하였다.

주요어: 접착강도, 박막시스템, 복합경도, 구속효과, 계면 물성, 계면 구속, 나노압입시험

학번: 2010-23197

List of Publications

I. International Journals

1. Seung-Kyun Kang, Young-Cheon Kim, Jinwoo Lee, Dongil Kwon, Ju-Young Kim: “Effect of contact angle on contact morphology and Vickers hardness measurement in instrumented indentation testing”, International Journal of Mechanical Sciences, Vol. 85, 104-109 (2014)

2. Jong-hyoung Kim, Jinwoo Lee, Woojoo Kim, Jongheon Kim, Seung-Kyun Kang, Dongil Kwon: “Characterization of viscoelastic behavior of Poly(dimethysiloxane) by nanoindentation”, KJMM, Vol. 57, 289-294 (2019)

3. Oh Min Kwon, Jiyeon Kim, Jinwoo Lee, Jong-hyoung Kim, Hee-Jun Ahn, Ju-Young Kim, Young-Cheon Kim, Dongil Kwon : “Compressive properties of nanoporous gold through

nanoindentation: an analytical approach based on the expanding cavity

model", Metals and Materials International, (2020)

II. International Conferences

1. Seung-Kyun Kang, Chan-Pyoung Park, Jinwoo Lee, Dongil Kwon: INVESTIGATING PILEUP OF METALLIC MATERIALS USING THE EQUIVALENT ELASTIC STRAINED VOLUME WITH EXPANDING CAVITY MODEL, IIW4, Seoul, Korea (2011)

2. Jongheon Kim, Jun-Yeong Kim, Jinwoo Lee, Dongil Kwon: Evaluation of Thin-film Interfacial Properties Using Indentation Test, PRICM 8, Hawaii, USA (2013)

3. Jongheon Kim, Sungki Choi, Jinwoo Lee, Dongil Kwon: Assessment of Interfacial Adhesion with the Nanoindentation Test, MRS, Boston, USA (2015)

4. Ju Yon Suh, Jinwoo Lee, Dongil Kwon: Evaluating the mechanical properties of polymeric materials using nanoindentation, IVC20, Busan, Korea (2016)

5. Jinwoo Lee, Ju Yon Suh, Jongho Won, Dongil Kwon: Evaluating the Adhesion Strength of Single Layered Thin Film deposited on the Metallic Substrate using Nano Indentation, ENGE 2016, Jeju, Korea (2016)

6. Jong-hyoung Kim, Jun Sang Lee, Hee-Jun Ahn, Oh Min Kwon, Jongho Won, Jinwoo Lee, Jeong Hwa Hong, Dongil Kwon: Estimation of Indentation load-depth curve of stress-free state from stressed state using the relationship between Indentation curve and Hardness, ACEM 2016, Jeju, Korea (2016)

7. Jinwoo Lee, Sungki Choi, Dongil Kwon: Evaluation of Thin-Film Interfacial properties using Single Nanoindentation Testing, IIW 6, Sapporo, Japan (2018)

8. Jinwoo Lee: Evaluation of Thin Film Interfacial Properties Using Single Nanoindentation Testing, ICMR 2019, Jeju, Korea (2019)

III. Domestic Conferences

1. 강승균, 박찬평, 이진우, 권동일: 소성쌓임 보정을 통한 압입 시험의 scaling relation 해석 및 압입각과 온도 의존성 규명, 2011년도 대한금속·재료학회 춘계 학술대회, 대구컨벤션센터(EXCO) (2011)

2. 전승원, 김준영, 이진우, 권동일: 구조용강의 파괴인성 천이거동 해석을 위한 연속압입시험의 응용, 2011년도 대한금속·재료학회 추계 학술대회, 대전컨벤션센터(DCC) (2011)

3. 권동일, 이규제, 이진우, 조원제: In-situ SEM indentation을 이용

한 Glass Frit material의 기계적 특성 예측 연구, 2012년도 대한금속·재료학회 춘계 학술대회, 현대성우리조트(강원도 횡성) (2012)

4. 이진우, 김준영, 조원제, 전승원, 권동일: 연속압입시험법을 이용한 금속재료의 샤르피 충격에너지 예측, 2012년도 대한금속·재료학회 춘계 학술대회, 현대성우리조트(강원도 횡성) (2012)

5. 김종헌, 이진우, 김인섭, 권동일: 압입시험을 이용한 박막의 계면 특성, 2012년도 대한금속·재료학회 추계 학술대회, 창원컨벤션센터 (2012)

6. 이진우, 조원제, 권동일: 연속압입시험을 활용한 OLED 패널의 접합부 충격특성 평가, 2014년도 대한금속·재료학회 춘계 학술대회, 대구컨벤션센터 (EXCO) (2014)

7. 이진우, 김종형, 김종헌, 권동일: 연속압입시험을 활용한 CIGS

박막태양전지의 복합환경 신뢰성 평가, 2014 Materials Fair, 서울대학교 (2014)

8. 이진우, 김종형, 김종헌, 권동일: 연속압입시험을 활용한 CIGS 박막태양전지의 복합환경 신뢰성 평가, 2014년도 대한금속·재료학회 추계 학술대회, 강원랜드 컨벤션호텔 (강원도 정선) (2014)

9. 김종헌, 최성기, 이진우, 권동일: Adhesion Evaluation Model of Thin Film Using Indentation, 2015년도 대한금속·재료학회 춘계 학술대회, 창원 컨벤션센터 (2015)

10. 서주연, 이진우, 김종헌, 권동일: The Adhesion Strength Evaluation Model of Thin Film Using Nano Indenation, 2016년도 대한금속·재료학회 춘계 학술대회, 경주화백컨벤션센터 (2016)

11. 이진우, 김종형, 김종헌, 임종경, 권동일: Evaluation of Thin

film Interfacial Properties using Single Nanoindentation Test, 2019년도 대한금속·재료학회 춘계 학술대회, 창원 컨벤션센터 (2019)